Estradiol elicits distinct firing patterns in arcuate nucleus kisspeptin neurons of females through altering ion channel conductances

Jian Qiu[1], Margaritis Voliotis[2,3], Martha A. Bosch[1], Xiao Feng Li[4], Larry S. Zweifel[5,6], Krasimira Tsaneva-Atanasova [2,3], Kevin T. O'Byrne[4] , Oline K. Rønnekleiv [1,7] and Martin J. Kelly [1,7]

[1]Department of Chemical Physiology and Biochemistry, Oregon Health and Science University, Portland, OR 97239, USA

[2]Department of Mathematics and Statistics, University of Exeter, Stocker Rd, Exeter, EX4 4PY, UK

[3]Living Systems Institute, University of Exeter, Stocker Rd, Exeter, EX4 4PY, UK

[4]Department of Women and Children's Health, School of Life Course and Population Sciences, King's College London, Guy's Campus, London SE1 1UL, UK

[5]Department of Psychiatry and Behavioral Sciences, University of Washington, Seattle, WA 98195, USA

[6]Depatment of Pharmacology, University of Washington, Seattle, WA 98195, USA

[7]Division of Neuroscience, Oregon National Primate Research Center, Beaverton, OR 97006, USA

Corresponding authors: Jian Qiu: qiuj@ohsu.edu; Martin J. Kelly: kellym@ohsu.edu

Competing Interest Statement: The authors have no competing interests to declare.

Abstract

Hypothalamic kisspeptin (Kiss1) neurons are vital for pubertal development and reproduction. Arcuate nucleus Kiss1 ($Kiss1^{ARH}$) neurons are responsible for the pulsatile release of Gonadotropin-releasing Hormone (GnRH). In females, the behavior of $Kiss1^{ARH}$ neurons, expressing Kiss1, Neurokinin B (NKB), and Dynorphin (Dyn), varies throughout the ovarian cycle. Studies indicate that 17β-estradiol (E2) reduces peptide expression but increases *Vglut2* mRNA and glutamate neurotransmission in these neurons, suggesting a shift from peptidergic to glutamatergic signaling. To investigate this shift, we combined transcriptomics, electrophysiology, and mathematical modeling. Our results demonstrate that E2 treatment upregulates the mRNA expression of voltage-activated calcium channels, elevating the whole-cell calcium current and that contribute to high-frequency burst firing. Additionally, E2 treatment decreased the mRNA levels of Canonical Transient Receptor Potential (TPRC) 5 and G protein-coupled K^+ (GIRK) channels. When TRPC5 channels in $Kiss1^{ARH}$ neurons were deleted using CRISPR, the slow excitatory postsynaptic potential (sEPSP) was eliminated. Our data enabled us to formulate a biophysically realistic mathematical model of the $Kiss1^{ARH}$ neuron, suggesting that E2 modifies ionic conductances in $Kiss1^{ARH}$ neurons, enabling the transition from high frequency synchronous firing through NKB-driven activation of TRPC5 channels to a short bursting mode facilitating glutamate release. In a low E2 milieu, synchronous firing of $Kiss1^{ARH}$ neurons drives pulsatile release of GnRH, while the transition to burst firing with high, preovulatory levels of E2 would facilitate the GnRH surge through its glutamatergic synaptic connection to preoptic Kiss1 neurons.

Keywords: Kisspeptin; Arcuate nucleus; 17β-estradiol; Ion channels; Synchronous firing; Burst firing; Mathematical modeling

Introduction

Hypothalamic kisspeptin (Kiss1) neurons and its cognate receptor (GPR 54 or Kiss1 R) are essential for pubertal development and reproduction, and may also be involved in the control of energy homeostasis (Kotani et al., 2001) (De Roux et al., 2003) (Seminara et al., 2003) (Messager et al., 2005) (Shahab et al., 2005) (d'Anglemont de Tassigny et al., 2008) (Qiu J. et al., 2018) (Rønnekleiv et al., 2022). Kisspeptin neurons within the arcuate nucleus of the hypothalamus ($Kiss1^{ARH}$) co-express Kiss1, Neurokinin B (NKB) and Dynorphin (Dyn), which are all down-regulated by 17β-estradiol (E2) (Goodman et al., 2007; Navarro V. M. et al., 2009). However, $Kiss1^{ARH}$ neurons also express vesicular glutamate transporter 2 (vGlut2) and release glutamate, and both vGlut2 expression and glutamate release are upregulated by E2 in females (Qiu J. et al., 2018). This indicates that peptides and glutamate in $Kiss1^{ARH}$ neurons are differently modulated by E2 and suggests that there is a complex E2 regulation in these neurons such that they transition from predominantly peptidergic to glutamatergic neurotransmission and hence from a “pulsatile” to “surge” mode. It has been known for decades that neurons located within the arcuate nucleus are responsible for the pulsatile release of GnRH and subsequently pulsatile release of LH from the pituitary gland (O'Byrne et al., 1991) (Moenter et al., 1993). In this respect, it is now generally accepted that $Kiss1^{ARH}$ neurons are the main neurons responsible for the generation of pulsatile LH release, but the underlying cellular conductances generating this activity have not been elucidated.

Morphological studies have provided evidence that $Kiss1^{ARH}$ neurons can communicate directly with each other (Lehman et al., 2010) (Navarro V. M. et al., 2009) (Navarro V.M. et al., 2011). Furthermore, $Kiss1^{ARH}$ neurons express the NKB receptor, Tacr3, as well as the kappa (κ) opioid receptor (KOR), whereas GPR54 is not expressed in $Kiss1^{ARH}$ neurons, rendering them unresponsive to kisspeptin (d'Anglemont de Tassigny et al., 2008; Navarro V. M. et al., 2009; Wakabayashi et al., 2010). Using optogenetics and whole-cell recordings we demonstrated that high-frequency photoactivation of $Kiss1^{ARH}$ neurons induces an NKB-mediated slow excitatory postsynaptic potential (EPSP), which is mediated by the recruitment of canonical transient receptor potential (TRCP5) channels. The release of NKB is limited by co-released dynorphin, which acts presynaptically to inhibit further release. Together the two peptides cause synchronized firing of $Kiss1^{ARH}$ neurons (Kelly et al., 2018; Qiu J. et al., 2016; Qiu Jian et al., 2021), whereas kisspeptin and glutamate appear to be the main output signals from $Kiss1^{ARH}$ neurons (Qiu J. et al., 2016; Qiu J. et al., 2018) (Voliotis et al., 2021) (Liu et al., 2021).

Although single action potential-generated calcium influx is sufficient to trigger the release of classical neurotransmitters such as glutamate, high frequency (10-20 Hz) is required for the release of neuropeptides such as kisspeptin, NKB and dynorphin (Qiu J. et al., 2016). Indeed, the slow EPSP, which underlies the synchronization, is similar to the “plateau potential” that has been described in hippocampal and cortical neurons (Arboit et al., 2020; Zhang Z. et al., 2011). Many neurons, including $Kiss1^{ARH}$ neurons, express the

biophysical properties that allow them to continue to persistently fire even after a triggering synaptic event has subsided (Zylberberg and Strowbridge, 2017) (Qiu J. et al., 2016). Moreover, the intrinsic bi-stability of neurons that generates persistent firing activity has been linked to a calcium-activated, non-selective cation current (I_{CAN}) (Zylberberg and Strowbridge, 2017), and TRPC channels, specifically TRPC5 channels, are thought to be responsible for the I_{CAN} in cortical neurons (Zhang Z. et al., 2011). Therefore, we postulated that TacR3 activation via NKB drives influx of Ca^{+2} through TRPC5 channels leading to greater build-up of $[Ca^{2+}]_i$ that facilitates the opening of more TRPC5 channels in a self-sustaining manner. Indeed, using the fast intracellular calcium chelator BAPTA, which has been shown to robustly inhibit TRPC5 channel activation in heterologous cells (Blair et al., 2009), we have been able to abolish the slow EPSP and persistent firing in $Kiss1^{ARH}$ neurons following optogenetic stimulation in female mice (Qiu Jian et al., 2021).

Although the expression of peptides in $Kiss1^{ARH}$ neurons are downregulated by high circulating levels (late follicular levels) of E2, the intrinsic excitability of and the glutamate release by $Kiss1^{ARH}$ neurons are increased by *Cacna1g* (Cav3.1, T-type calcium channel), *Hcn1* and *Hcn2* (Hyperpolarization-activated, Cyclic Nucleotide Gated channels) mRNA expression and *Vglut2* mRNA expression, respectively (Qiu J. et al., 2018). Burst firing in CNS neurons, which efficiently releases fast amino acid transmitters like glutamate, is generated primarily by the T-type calcium channel current (I_T) (*e.g.,* in thalamic relay neurons), and the rhythmicity of this burst firing is dependent on the h-current (I_h) (for review, see (Lüthi and McCormick, 1998; Zagotta and Siegelbaum, 1996)). I_h is mediated by the HCN channel family, which includes channel subtypes 1-4, of which *Hcn1* and *Hcn2* are the main channels in $Kiss1^{ARH}$ neurons. I_h depolarizes neurons from hyperpolarized states, raising the membrane potential into the range of I_T activation (Erickson et al., 1993a, 1993b; Kelly and Rønnekleiv, 1994; Lüthi and McCormick, 1998; Zhang C. et al., 2009). I_T is mediated by the low-threshold voltage-gated calcium channels, $Ca_V3.1$-3.3 (for review see (Perez-Reyes, 2003)). I_T initiates a transient Ca^{2+}-driven depolarization above the threshold for action potential initiation (*i.e*., a low threshold spike) (Llinás, 1988; Tsien et al., 1987). This depolarization then drives neurons to fire an ensemble (burst) of Na^+-driven action potentials.

Based on the above compelling evidence we postulated that $Kiss1^{ARH}$ neurons transition from peptidergic neurotransmission, driving the pulsatile release of GnRH via kisspeptin release into the median eminence, to glutamatergic transmission that facilitates in the preovulatory surge of GnRH (Lin et al., 2021) (Shen et al., 2022) through their projection to the anteroventral periventricular/periventricular nucleus Kiss1 ($Kiss1^{AVPV/PeN}$) neurons (Qiu J. et al., 2016). Therefore, we initiated studies to thoroughly characterize effects of high circulating (late follicular) levels of E2 on the expression of the full complement of voltage-activated calcium channels (and currents) and the opposing K^+ channels, involved in the repolarization, on the excitability of $Kiss1^{ARH}$ neurons. We performed whole-cell recordings and single cell RT- PCR analysis of $Kiss1^{ARH}$ neurons to determine which channels are involved in the physiological transition from peptidergic to glutamatergic neurotransmission. Our physiological findings were incorporated into a mathematical model that accounts for

the E2 effects on the firing activity of Kiss1^{ARH} neurons and validates our hypothesis that high levels of E2 facilitate the transition from peptidergic to glutamatergic neurotransmission.

Results

Voltage-activated Ca^{2+} channels contribute to burst firing of Kiss1^{ARH} neurons

Our whole-cell current clamp recordings of Kiss1^{ARH} neurons revealed that there is a significant transition of these Kiss1 neurons from a silent/tonic firing mode in the ovariectomized state to bursting/irregular firing with E2 treatment (**Figure 1**). Therefore, we sought to elucidate the cationic channels contributing to this physiological transition. Previously, we have shown that an increase in the intracellular calcium concentrations can potentiate TRPC5 channel current in POMC neurons (Qiu J. et al., 2010). Additionally, chelating intracellular calcium with BAPTA abolishes the slow excitatory postsynaptic potential (EPSP) and persistent firing in Kiss1^{ARH} neurons (Qiu Jian et al., 2021). Hence, to investigate the contributions of voltage-activated calcium channels (VGCCs) to the increase in intracellular calcium, we measured the peak calcium current contributed by both the low and high voltage-activated calcium channels. The inward currents evoked by the voltage pulses (150-ms pulses starting from a holding potential of -80 mV with 10-mV increments) were identified as calcium (Ca^{2+}) currents, as they were blocked by the universal VGCC inhibitor Cd^{2+} (200 μM) (McNally et al., 2020) (**Figures 2A-E**). The maximum total inward and Cd^{2+}-sensitive currents reached their peak amplitudes at -10 mV. To differentiate between various calcium channel subtypes present in Kiss1^{ARH} neurons, we applied selective antagonists individually, allowing us to isolate the drug-sensitive current for each cell. When we individually applied specific antagonists, we observed partial inhibition of whole-cell Ca^{2+} currents. Treatment with 10 μM nifedipine (Hiraizumi et al., 2008; Kato et al., 2003; Lee et al., 2002), an L-type Ca^{2+} channel inhibitor, resulted in a partial inhibition (26.1%) of the whole-cell calcium current. Additionally, application of 2 μM ω-conotoxin GVIA (conoGVIA, targeting N-type channels) (Lee et al., 2002), 200 nM ω-agatoxin IVA (AgaIVA, targeting P/Q-type channels) (Kato et al., 2003; McNally et al., 2020), 100 nM SNX-482 (targeting R-type channels) (Hiraizumi et al., 2008), or 1 μM TTA-P2 (TTAP2, targeting T-type channels) (McNally et al., 2020) also led to partial inhibition of the Ca^{2+} current (**Figure 2F**). The observed reduction in current with each inhibitor indicates the presence of all the major subtypes of Ca^{2+} currents in Kiss1^{ARH} neurons. Among the inhibitors used, the largest components of the whole-cell calcium current were sensitive to nifedipine (26.1%), conoGVIA (25.1%), and SNX-482 (31.1%) (**Figures 2A, B, D and 2F**). Subsequently, we documented contributions from TTA-P2-sensitive channels, accounting for approximately 6.7% of the total Ca^{2+} current, and AgaIVA-sensitive channels, which constituted approximately 3.9% (**Figures 2E, C**). These findings indicate that high voltage-activated L-, N-, and R-type channels constitute the largest component of the voltage-activated Ca^{2+} current in Kiss1^{ARH} neurons that not only increases the overall excitability but also greatly facilitate TRPC5 channel opening (Blair et al., 2009), which is the major downstream target of TACR3 activation by NKB (Qiu J. et al., 2016).

Voltage-activated Ca^{2+} channels contribute to generation of slow-EPSP in $Kiss1^{ARH}$ neurons

Our previous study utilizing optogenetics demonstrated that high frequency photostimulation of $Kiss1^{ARH}$ neurons releases NKB. This release of NKB induces slow excitatory postsynaptic potentials (EPSPs) that facilitate the recruitment of other $Kiss1^{ARH}$ neurons, resulting in synchronous firing of the $Kiss1^{ARH}$ neuronal population (Qiu J. et al., 2016). Additionally, chelating intracellular calcium with the fast chelator BAPTA abolishes the slow EPSP and persistent firing in $Kiss1^{ARH}$ neurons, highlighting the role of calcium signaling in these processes (Qiu Jian et al., 2021). To access the involvement of HVA channels in the generation of the slow EPSP, we conducted experiments where we blocked the L-type Ca^{2+} channels with nifedipine (10 μM) and the N- and P/Q-type Ca^{2+} channels with ω-conotoxin MVIIC (1 μM) (Nunemaker et al., 2003). We then measured the slow EPSP. Indeed, both nifedipine and ω-conotoxin MVIIC significantly inhibited the slow EPSP by 35.2% and 60.4%, respectively (**Figure 3A, B, E**). In addition, we used SNX (100 nM), which selectively blocks R-type Ca^{2+} channels, and the slow EPSP was reduced to 28.7% of its control value (**Figure 3C, E**). The selective T-channel blocker TTA-P2 (5 μM) inhibited the slow EPSP by 28.6% (**Figure 3D, E**). Since the pharmacological blockade of the various calcium channels could also affect the presynaptic release of neurotransmitters (*i.e.,* NKB), we measured the direct response of $Kiss1^{ARH}$ neurons to the TACR3 agonist senktide in the presence or absence of cadmium, a universal calcium channel blocker (**Figures 3F-H**). Indeed, Cd^{2+} significantly inhibited the inward current induced by senktide, which supports our posit that the plasma membrane calcium channels contribute to the TRPC5 channels activation. Therefore, it appears that calcium channels contribute to maintaining the sustained depolarization underlying the slow EPSP.

E2 increases the mRNA expression and the whole-cell current of voltage-activated Ca^{2+} channels

The neuropeptides NKB (tachykinin2, *Tac2*) and kisspeptin (*Kiss1*), which are expressed in $Kiss1^{ARH}$ neurons, are crucial for the pulsatile release of gonadotropin-releasing hormone (GnRH) and reproductive processes. E2 decreases the expression of *Kiss1* and *Tac2* mRNA in $Kiss1^{ARH}$ neurons but enhances the excitability of $Kiss1^{ARH}$ neurons by amplifying the expression of *Cacna1g*, *Hcn1*, and *Hcn2* mRNA, as well as increasing T-type calcium currents and h-currents, respectively (Qiu, 2018, 20613}. Moreover, E2 drives *Slc17a6* mRNA expression and enhances glutamatergic synaptic input to arcuate neurons and $Kiss1^{AVPV/PeN}$ neurons (Qiu J. et al., 2018). As a result, the E2-driven increase in $Kiss1^{ARH}$ neuronal excitability and glutamate neurotransmission may play a crucial role in triggering the surge of GnRH, ultimately leading to the LH surge (Lin et al., 2021) (Shen et al., 2022).

To assess the impact of E2 on the modulation of voltage-activated calcium channels and $Kiss1^{ARH}$ neuronal excitability, we employed real-time PCR (qPCR) to measure the relative expression levels of ion channel subtypes in $Kiss1^{ARH}$ neurons. We compared the expression in E2-treated females to those treated with oil,

using the specific primers listed in Table 1. The quantification was conducted on pools of 10 neurons, as indicated in the Methods and Materials. In both oil- and E2-treated females, we quantified the expression of *Cav1.2* (L-type), *Cav2.1* (P/Q-type), *Cav2.2* (N-type) and *Cav2.3* (R-type) mRNAs. Remarkably, all of these mRNA transcripts exhibited increased expression levels in response to E2 treatment (**Figure 4**). Congruent with our previous findings (Qiu J. et al., 2018), we observed that the mRNA expression of *Cav3.1 and Hcn1* was also upregulated in response to E2 treatment (**Figure 4**). These results suggested that E2 has a regulatory effect on the expression and function of all of these ion channels in $Kiss1^{ARH}$ neurons. To determine whether the increased mRNA expression translated into functional changes at the cellular level, we measured the whole-cell calcium current in $Kiss1^{ARH}$ neurons obtained from ovariectomized mice treated with either vehicle or E2. We discovered that E2 treatment led to a significant increase in the peak calcium current density in $Kiss1^{ARH}$ neurons (**Figure 5A-D**), which was recapitulated by our computational modeling (**Figure 5E**). These findings indicate that the upregulation of the mRNA expression of calcium channels by E2 translated to an augmented peak calcium current in $Kiss1^{ARH}$ neurons.

The largest components of the calcium currents in $Kiss1^{ARH}$ neurons from the E2-treated, ovariectomized females were found to be sensitive to nifedipine, conoGVIA, and SNX-482, accounting for approximately 24.9%, 24.6%, and 27.0% of the total current across cells, respectively, which is very similar to their contributions to the whole-cell current from vehicle-treated, ovariectomized females (**Figure 3**). In addition, contributions from TTA-P2-sensitive channels accounted for approximately 11.1% of the total Ca^{2+} current, while agaIVA-sensitive channels contributed to approximately 11.0% (**Figure 5D**). These results highlight the prevalence of L-, N-, and R-type calcium channels as the major contributors to the whole-cell calcium current in $Kiss1^{ARH}$ neurons from E2-treated, ovariectomized females, but also the involvement of T-type and P/Q-type channels.

E2 does not alter the kinetics of calcium channel activation or de-inactivation

In order to determine whether the increase in peak voltage-activated calcium current density was the result of E2 regulating calcium channel kinetics, mRNA expression or both, we examined the voltage dependence of activation and inactivation. By measuring the voltage dependence of activation, we assessed how E2 affects the ability of calcium channels to open in response to membrane potential changes. Similarly, by examining the voltage dependence of inactivation, we determined how E2 influences the inactivation kinetics of calcium channels. Based on our results, there was no difference in the voltage dependence of activation between cells from the vehicle-treated control group ($V_{1/2}$ = -32.3 ± 2.1 mV; n = 13) and cells from estrogen-treated females ($V_{1/2}$ = -33.6 ± 2.5 mV; n = 11). Similarly, there was not a significant difference in the voltage dependence of inactivation between control cells ($V_{1/2}$ = -48.9 ± 4.8 mV; n = 6) and estrogen-treated cells ($V_{1/2}$ = -44.1 ± 1.9 mV; n = 5) (**Figure 6**). Therefore, although long-term E2 treatment increased the mRNA expression of HVA

calcium channels (**Figure 4**), it did not affect the channel kinetics in Kiss1^{ARH} neurons (**Figure 6**). Also, E2 downregulated the expression of *Kcnd2* mRNA encoding Kv4.2, which is expressed in Kiss1^{ARH} neurons (Mendonça et al., 2018) and has similar kinetics of activation as the T-type calcium channels (Oil-treated, ovariectomized females relative mRNA expression: 1.053, n = 5 animals versus E2-treated expression: 0.5643, n=5; t-test p = 0.0061). This opposing K^+ current would dampen the inward calcium current. Therefore, it appears that long-term E2 treatment does not modulate calcium channel kinetics but rather alters the mRNA expression to increase the calcium channel conductance.

BK, SK and KCNQ channels are involved in modulating excitability of Kiss1^{ARH} neurons

In the brain, calcium plays a crucial role in sculpting neuronal firing by activating potassium channels, which subsequently influence neuronal behavior (Nicoll, 1988; Storm, 1990). Since HVA and LVA calcium channels were expressed in Kiss1^{ARH} neurons, all of which contribute to the elevation of intracellular calcium concentration ($[Ca^{2+}]_i$) that facilitates TRPC5 channel opening (Blair et al., 2009), our next step involved measuring the changes in Ca^{2+}-activated K^+ channel conductances and assessing their mRNA expression. In various cell types increases in cytosolic calcium levels, whether resulting from extracellular influx or intracellular release, lead to the activation of plasma membrane calcium-dependent potassium channels (Sah Pankaj and Louise Faber, 2002). Similarly, in Kiss1^{ARH} neurons, these channels would be activated by calcium influx through all four types of high voltage-gated calcium channels, as well as the low voltage-activated calcium channel, which are all active during action potential firing. The activity of Ca^{2+}-activated K^+ channels play a crucial role in numerous physiological processes, including secretion and the regulation of neuronal firing properties. Two main families of Ca^{2+}-activated K^+ channel channels have been characterized, distinguished by their biophysical and pharmacological properties. These families are known as BK (Big Conductance K^+) and SK (Small Conductance K^+) channels in the CNS (Kshatri et al., 2018). BK channels are known for their high potassium selectivity and large single channel conductance, typically ranging from 100 to 300 pS. Activation of BK channels requires both calcium binding and membrane depolarization (Blatz and Magleby, 1987; Marty, 1989; Sah P., 1996; Storm, 1990). On the other hand, SK channels are simply activated by increases in cytosolic calcium levels, with their half-maximal activation at 0.3 μM (Bond et al., 1999).

To investigate K^+ currents, the cells were maintained at a holding potential of -70 mV while being exposed to blockers CNQX, AP5, picrotoxin and TTX. Subsequently, the membrane potential was stepped by depolarizing voltages, ranging from -60 mV to +40 mV in 10 mV increments, for a duration of 500 ms (Brereton et al., 2013). This protocol was employed to activate K^+ currents (**Figure 7A**). First, we examined SK currents. The mean current density was determined at the end of the voltage pulses. In vehicle-treated, OVX females the application of the SK channel blocker apamin (100 nM) (Spergel, 2007) led to a significant reduction in whole-cell currents in the +10 to +40 mV range (**Figures 7A, B**). The mean outward current density at +40 mV in the

control group was 125.5 ± 7.2 pA/pF (n = 5) with the apamin-sensitive component contributing 60.2 ± 3.3 pA/pF (n = 5) (**Figures 7A, C**). In contrast, in the E2-treated females, the overall mean outward current density at +40 mV was 195.4 ± 14.6 pA/pF (n = 6), which was significantly greater than the vehicle control group (**Figures 7D, E**). However, there was no significant difference in the apamin-sensitive component between the vehicle-treated and E2-treated females, 60.2 ± 3.3 pA/pF (n = 5) versus 128.1 ± 13 pA/pF (n = 6), respectively (**Figure 7F**). Furthermore, to investigate the expression of the mRNAs encoding SK channel subunits in $Kiss1^{ARH}$ neurons from vehicle-treated and E2-treated OVX females, qPCR experiments were performed on 10-cell $Kiss1^{ARH}$ neuronal pools (**Figure 7G**). We focused on SK3 channels because these channels exhibit the highest expression in the hypothalamus and E2 regulates their expression (Bosch et al., 2002). E2 treatment had no effect on the mRNA expression of the *SK3* subunit. These molecular findings support our electrophysiology results. Our computational model was calibrated so that SK channels contributed ~50 pA/pF to the whole-cell outward K^+ current in E2-treated females (**Figure 7H**).

Additionally, following the same protocol and in the presence of the same cocktail of blockers (CNQX, AP5, picrotoxin and TTX), we investigated the contribution of BK channels to $Kiss1^{ARH}$ neuronal excitability. In the OVX females, the application of the BK channel blocker iberiotoxin (ibTx, 200 nM) (Niday and Bean, 2021) resulted in only a slight attenuation of the outward current (n = 5) (**Figures 8A, B**). The ibTx-sensitive current density measured at +40 mV was 32.8 ± 12.0 pA/pF (**Figures 8A, C**). However, in the E2-treated females, the application of ibTx significantly attenuated the whole-cell K^+ current from +20 to +40 mV, (**Figures 8D, E**). Additionally, the ibTx-sensitive current was significantly larger in the +0 to +40 mV range in the E2-treated females compared to the OVX females (**Figure 8F**). These findings indicate that E2 treatment modulates the activity of ibTx-sensitive BK current in $Kiss1^{ARH}$ neurons, resulting in increased current density (90.0 ± 10.1 pA/pF (n = 6) versus 31.1 ± 8.4 pA/pF (n = 5) at +40 mV). To investigate the expression of mRNA encoding BK channel subunits in $Kiss1^{ARH}$ neurons from vehicle-treated and E2-treated OVX females, qPCR experiments were performed on 10-cell $Kiss1^{ARH}$ neuronal pools (**Figure 8G**). E2 treatment significantly increased the mRNA expression of the BKα1 (*Kcnma1*) subunit. These findings support our electrophysiological findings that there is a significant increase in BK channel activity in $Kiss1^{ARH}$ neurons with E2 treatment (**Figure 8F**). In addition, E2 increased the mRNA expression of *Kcnb1* encoding delayed rectifier Kv2.1 (E2-treated relative mRNA expression: 1.672, n = 5 versus oil-treated mRNA expression: 1.086, n = 5; t-test p-value = 0.0024). The up-regulation of the two of these K^+ channels (BKα1 and Kv2.1) would facilitate rapid repolarization of $Kiss1^{ARH}$ following an action potential. Our computational model was calibrated so that BK channels contributed ~100 pA/pF to the whole cell outward K^+ current in the E2-treated females (**Figures 8H**).

Traditionally, the after hyperpolarization is divided into three distinct phases: fast (fAHP), medium (mAHP), and slow after hyperpolarization (sAHP) (Storm, 1990; Vogalis et al., 2003). The fast after hyperpolarization (fAHP) is primarily mediated by the BK family of potassium channels (Storm, 1987). The medium after hyperpolarization (mAHP) is predominantly mediated by apamin-sensitive SK2 channels (Bond et al., 2004;

Peters et al., 2005). However, KCNQ family members contribute to both the mAHP and sAHP (Tzingounis A. V. et al., 2010; Tzingounis A. V. and Nicoll, 2008). Therefore, to investigate the contribution of KCNQ channels to Kiss1^{ARH} neuronal excitability, voltage clamp experiments were conducted in the presence of TTX, CNQX, AP5, and picrotoxin, and a standard M-current protocol was run using the M-channel blocker XE-991 to isolate the M-current (Greene et al., 2017; Roepke et al., 2011) (**Figure 9 A, B**). The application of XE-991 resulted in the inhibition of M-current within a physiologically relevant voltage range of -60 to -30 mV in E2-treated OVX females but exhibited minimal impact in OVX females (**Figure 9 C, D**). Although the XE991-sensitive current was relatively small compared to other voltage-activated K^+ conductances, it demonstrated a significant increase in E2-treated, OVX females (**Figures 9 E**). The maximum peak current density sensitive to XE-991 at -30 mV was found to be four times higher in E2-treated OVX females when compared to OVX females. This would contribute to the repolarization following burst firing. Furthermore, E2 increased the mRNA expression of *Kcnq2*, (**Figure 9F**), which suggests that KCNQ channels play a role in repolarizing Kiss1^{ARH} neurons following burst firing. Indeed, our modeling predicted that M-current contributed to the repolarization following burst firing (**Figure 9G**).

E2 increases Vglut2 but down regulates Tac2, Trpc5 and Girk2 mRNA expression in Kiss1^{ARH} neurons

Based on our electrophysiological results, Kiss1^{ARH} neurons appear to transition from peptidergic to glutamatergic neurotransmission through E2-mediated changes in the expression of voltage-activated Ca^{2+} channels and K^+ channels and their respective conductances. Therefore, we asked the question is there a difference in peptide and glutamate mRNA expression mediating this transition? Therefore, we ran a comparison between *Tac 2* (NKB) and *Vglut2* (surrogate for glutamate) expression. The cycle threshold (CT) was compared between *Tac2* and *Vglut2* as well as *Kiss1*, *TRPC5* and *GIRK2* in Kiss neuronal cell pools from OVX oil-treated and OVX E2-treated animals (**Figures 10A, B**). It is worth noting that lower number of cycles illustrate a higher quantity of mRNA expression because the fluorescence is detected earlier, and one cycle difference represents a doubling in expression. As expected, the reference gene *Gapdh* did not change with E2-treatment. However, quantitative PCR results revealed that E2 treatment of OVX females significantly reduced *Tac2* expression (**Figure 10C**), whereas *Vglut2* mRNA was significantly increased in Kiss1^{ARH} neurons (**Figure 10D**). Moreover, both *Trpc5* and *Girk2* expression were significantly reduced in E2-treated, OVX females (**Figures 10E, F)**.

CRISPR mutagenesis of Trpc5 attenuates slow EPSP and reduces excitability of Kiss1^{ARH} neurons

Our previous (Qiu Jian et al., 2021) and current findings suggested that TRPC5 channels play a dominant role in regulating cell excitability in ovariectomized females. Therefore, as proof of principle, we utilized a CRISPR approach to mutate TRPC5 channels in Kiss1^{ARH} neurons similar to our previous studies (Hunker et al., 2020;

Stincic et al., 2021). Hunker *et al*. developed a single viral vector for conditional expression of the smaller *Staphylococcus aureus* (SaCas9) and sgRNA that yields high-efficiency mutagenesis in specific cell types (Hunker et al., 2020). To selectively mutate *Trpc5* in Kiss1^{ARH} neurons, we generated two guide RNA's, one targeting exon 2, which is conserved across all splice variants, and the other targeting exon 7, the pore forming domain (**Figures 11A, B**). A cohort of Kiss1^{ARH} mice were given bilateral stereotaxic injections into the ARH of the two AAV1-FLEX-SaCas9-sgTrpc5's or a control virus containing with AAV1-FLEX-SaCas9-U6-sg*Rosa26*. An additional Cre-dependent virus of the same serotype (AAV1) that drove expression of a fluorophore (YFP or mCherry) was co-administered in order to visualize injection quality and facilitate harvesting of cells (**Figure 11C**). After three weeks, mice underwent ovariectomy since OVX mice express the maximum slow EPSP amplitude (Qiu J. et al., 2016). Brain slices were prepared, and cells harvested as previously described (Qiu J. et al., 2018) and analyzed with qPCR. We found that the *Trpc5* mutagenesis group displayed a reduction in relative expression of *Trpc5* in Kiss1^{ARH} neurons compared to the control group (**Figure 11D**). Hence, the qPCR data verified that in the *sgTrpc5*-targeted mice we can selectively reduce *Trpc5* gene expression in targeted cells.

As predicted, mutagenesis of Trpc5 channels in Kiss1^{ARH} neurons significantly attenuated the slow EPSP (**Figures 12A, B, C**) such that the postsynaptic excitation was reduced to a "trickle" of action potential firing. What we would not have predicted is that the double sgRNA mutagenesis of *Trpc5* channels in Kiss1^{ARH} neurons significantly hyperpolarized the resting membrane potential by 7 mV (**Figure 12D**). Moreover, the rheobase (minimum current required to induce firing) significantly increased by ~13 % in females bearing the *sgTrpc5* double mutagenesis (**Figure 12E**). The firing frequency versus injected current (F-I) curve for sg*Trpc5* double mutagenesis Kiss1^{ARH} neurons was also significantly attenuated (**Figure 12F**). In agreement with these experimental findings, current ramp simulations of our mathematical model confirmed that a decrease of the TPRC5 conductance increased the rheobase and reduce the firing activity of Kiss1^{ARH} neurons (**Figures 12G, H**). In our model, this contribution of TRPC5 channels to cell excitability is attributed to intracellular calcium levels which activate TRPC5 channels independently of NKB stimulation. Finally, we employed our mathematical model to further investigate the transition from synchronous firing driven by NKB release and TRPC5 channel activation to burst firing generated by E2-mediated upregulation of endogenous conductances. As we varied the conductance of TRCP5 channels and GIRK channels under saturating extracellular signals (*e.g.*, NKB and Dyn), we find that balance between the two conductances controls the neuronal excitability in the OVX parameterized model, with synchronous firing eliminated when TRPC5 conductance is low (red triangle) relative to the GIRK conductance (**Figure 13A**). Furthermore, the burst firing of the OVX+E2 parameterized model was supported by elevated h- and Ca^{2+}-currents (**Figure 13B**) as well as by the high conductance of Ca^{2+} channels relative to the conductance of TRPC5 channels (**Figure 13C**). Importantly, the simulated burst firing was analogous to the phasic burst firing recorded *ex vivo* in Kiss1^{ARH} neurons (**Figure 1A**).

Discussion

E2 appears to play a critical role in transitioning the glutamatergic/peptidergic Kiss1^{ARH} neurons from a high frequency firing mode during synchronization, which is dependent on NKB-driven activation of TRPC5 channels, to a short bursting mode that would facilitate glutamate release. E2 decreased the expression of the peptide neurotransmitters NKB (kisspeptin and dynorphin) and TRPC5 channels but increased the mRNA expression of *Vglut2,* voltage-activated calcium channels and *Hcn* channels that contribute to burst firing and glutamate release from the Kiss1^{ARH} neurons. We determined that the increase in mRNA expression of the HVA calcium channels translated into a significant increase in whole-cell current with all of the calcium channels contributing proportionally. Most importantly the kinetics of activation and inactivation were unaltered with E2 treatment, which indicates that other post-translation modifications were not affecting channel activity. Surprisingly and somewhat counter intuitive, the *BK α1* subunit was also upregulated, but based on our modeling the rapid repolarization of the Kiss1^{ARH} neurons (*i.e.,* the fast AHP) would facilitate higher frequency of action potential firing. Moreover, our modeling confirmed that TRPC5 channels, which generate the slow EPSP (*a.k.a*., plateau potential in other CNS neurons), are vital for initiating and sustaining synchronous firing of Kiss1^{ARH} neurons, while subsequent activation of GIRK channels repolarizes Kiss1^{ARH} neurons. E2 treatment of ovariectomized females decreased both *Trpc5* and *Girk2* channel mRNA expression, which in our model correlated with the reduction in sustained high frequency firing of Kiss1^{ARH} neurons. Therefore, the synchronous high frequency firing of Kiss1^{ARH} neurons in a low E2 milieu correlates with the pulsatile release of GnRH (LH from the pituitary gland), whereas the transition to burst firing in the presence of high circulating levels of E2 (*e.g*., proestrus) would facilitate the GnRH (LH) surge through its glutamatergic synaptic connection with Kiss1$^{AVPV/PeN}$ neurons (Lin et al., 2021; Qiu J. et al., 2016).

Core calcium conductances underlying synchronous and burst firing of Kiss1^{ARH} neurons

TRPC5 channels are highly expressed in Kiss1^{ARH} neurons (**Figure 11**), and TRPC5 channels are essentially ligand-activated calcium channels with a high permeability to calcium (P_{Ca}/P_{Na} = 9:1) (Venkatachalam and Montell, 2007). In general, mammalian TRPC channels are activated by both G protein-coupled receptors and receptor tyrosine kinases (Ambudkar and Ong, 2007; Clapham, 2003), and are one of the major downstream effectors activated by glutamate binding to group I metabotropic glutamate receptors (mGluR1 and mGluR5) in CNS neurons (Bengtson et al., 2004; Berg et al., 2007; Faber et al., 2006; Tozzi et al., 2003). In substantia nigra dopamine neurons mGluR1 agonists induce a current that exhibits the tell-tale double-rectifying current-voltage plot of TRPC channel activation (Tozzi et al., 2003), similar to what we see with the effects of the NKB agonist senktide in Kiss1^{ARH} neurons (Qiu Jian et al., 2021). Both mGluR1 and TacR3 are Gq-coupled to phospholipase C (PLC) activation which leads to hydrolysis of phosphatidylinositol 4,5-bisphosphate (PIP_2) to

diacylglycerol (DAG) and inositol 1,4,5 triphosphate (IP_3), which is involved in channel activation (Birnbaumer, 2009). TacR3 (NKB) signaling has additional consequences since many K^+ (e.g., GIRK, KCNQ) channels are dependent on PIP2 for channel opening, and depletion of PIP2 by PLC leads to channel closure (Brown and Passmore, 2009) (Zhang C. et al., 2013) (Whorton and MacKinnon, 2011) (Zheng et al., 2022). Therefore, depletion of PIP2 by NKB signaling would further facilitate the sustained firing of $Kiss1^{ARH}$ neurons during synchronization.

A plateau potential has been characterized in hippocampal and cortical neurons (Arboit et al., 2020; Zhang Z. et al., 2011) as such these neurons express biophysical properties that allow them to continue to persistently fire even after a triggering synaptic event has subsided (Zylberberg and Strowbridge, 2017). The persistent firing activity of these neurons is linked to I_{CAN} (Zylberberg and Strowbridge, 2017), and TRPC5 channels appear to be responsible for the I_{CAN} (Zhang Z. et al., 2011). With TacR3 activation in $Kiss1^{ARH}$ neurons there is an influx of Ca^{+2} through TRPC5 channels leading to greater build-up of $[Ca^{2+}]_i$ that facilitates the opening of more TRPC5 channels in a self-sustaining (autocatalytic) manner (Qiu J. et al., 2016). Using the fast intracellular calcium chelator BAPTA, which has been shown to robustly inhibit TRPC5 channel activation in heterologous cells (Blair et al., 2009), we abolished the slow EPSP and persistent firing of $Kiss1^{ARH}$ neurons following optogenetic stimulation (Qiu Jian et al., 2021). Moreover, HVA calcium channel blockers attenuated the generation of the slow EPSP (**Figure 3**) so it appears that they also contribute to the I_{CAN} since calcium influx via both LVA and HVA calcium channels can also facilitate TRPC5 channel opening in $Kiss1^{ARH}$ neurons. In the ovariectomized female, treatment with E2 upregulated *Cav1.2, Cav2.1, Cav2.2, and Cav2.3 mRNA by 1.5- to 2-fold and Cav3.1* mRNA expression by ~3-fold. Hence, E2 significantly increased whole-cell calcium currents $Kiss1^{ARH}$ neurons, which greatly enhanced the excitability and contributed to the burst firing of $Kiss1^{ARH}$ neurons (**Figure 1**). However, the amplitude of the slow EPSP with E2 treatment is only ~25% of the amplitude in the ovariectomized state (Qiu J. et al., 2016). Therefore, there appears to be a physiologic transition of $Kiss1^{ARH}$ neurons from the slow EPSP firing mode in the OVX state to the burst firing mode in the presence of E2, which has important physiologic ramifications as discussed below.

TRPC5 and GIRK channels are vital for synchronization of $Kiss1^{ARH}$ neurons

Recently, Tian *et al*. demonstrated that TRPC4, a close homolog of TRPC5 sharing ~64 percent homology, is a “coincidence detector” of neurotransmission by both Gq/11 and Gi/o-coupled receptors in lateral septal (LS) neurons (Tian et al., 2022). In whole-cell recordings of LS neurons, TRPC 4 channels mediate a strong depolarizing plateau potential that in contrast to TRPC5 channel activation in $Kiss1^{ARH}$ neurons, abrogates action potential firing as a result of a depolarization block. In many instances the plateau potential in LS neurons is followed by an AHP, which is dependent on the activation of Gi/o-coupled receptors. In contrast, we have not observed an AHP in $Kiss1^{ARH}$ neurons following the slow EPSP (Qiu J. et al., 2016). Tian and

colleagues showed that the depolarizing plateau in LS neurons is codependent on activation of both Gq/11-coupled mGluR1 glutamate receptors and Gi/o-coupled γ-aminobutyric acid type B receptors, the latter activating GIRK channels. Moreover, the firing patterns in LS neurons encodes information about the relative strengths of these contrasting inputs (*i.e.,* Gq/11 versus Gi/o) such that only mGluR1 produces weak depolarization accompanied by increased firing of LS neurons, whereas pure $GABA_B$ receptor activation hyperpolarizes the cells and abrogates firing activity. Coincident input of both mGluR1 and $GABA_B$ receptors results in a brief burst of action potentials followed by a pause in firing, and both the pause duration and firing recovery patterns reflect the relative strengths of Gq/11 versus Gi/o inputs. Importantly, Tian and colleagues computationally simulated these various scenarios with computational modeling, and similar to our modeling, utilized only TRPC4 and GIRK channels. A notable difference between the $Kiss1^{ARH}$ neurons and the LS neurons is that dynorphin binds to kappa-opioid receptors to open GIRK channels in the nerve terminal of $Kiss1^{ARH}$ neurons (presynaptic effect) (Qiu J. et al., 2016), whereas GABA binds to some $GABA_B$ receptors to hyperpolarize LS neurons (Tian et al., 2022). Therefore, although the high frequency firing activity of both LS and $Kiss1^{ARH}$ neurons can be modeled around TRPC and GIRK channels, the generated firing patterns are dramatically different based on the timing (co-incident activation of TRPC4 and GIRK channels in LS) and localization of the kappa opioid-coupled GIRK channels in the axon terminal of $Kiss1^{ARH}$ neurons. Moreover, E2-treated, ovariectomized females show a significant down-regulation of both *Trpc5 and Girk2* mRNA expression in $Kiss1^{ARH}$ neurons (**Figure 10**), which is important for the physiological transitioning as described below.

Interestingly, the hypothalamic A12 (ARH) dopamine neurons show a rhythmic “oscillatory” firing behavior that transitions to a tonic firing mode with synaptic input from Thyrotropin-releasing hormone (TRH) neurons (Lyons D.J. et al., 2010) or feedback by circulating prolactin, released by pituitary lactotrophs (Lyons D. J. et al., 2012). A more recent paper has revealed that TRPC5 channels mediate the plateau potential and tonic firing in A12 dopamine neurons in response to prolactin (Blum et al., 2019). Similar to our findings with CRISPR deletion of Trpc5 in $Kiss1^{ARH}$ neurons (**Figures 11 and 12**), conditional knockout of Trpc5 in dopamine neurons abrogated the prolactin-induced plateau potential and tonic firing. Although Blum and colleagues did not model the oscillatory firing or tonic firing of the A12 dopamine neurons, their findings are consistent with our results showing that the activation of TRPC5 channels underlies the slow EPSP (plateau potential) and sustained firing.

Contribution of endogenous K^+ channels to synchronized and burst firing

Beyond the ligand-gated (*e.g.,* baclofen) GIRK channels, there are endogenous K^+ channels that help sculpt the firing activity of kisspeptin neurons. We focused on the calcium-activated K^+ channel family: the large-conductance, calcium-activated potassium (BK, also called BK_{Ca}, $K_{Ca}1.1$, MaxiK, *Slo*), small conductance,

calcium-activated K^+ (SK1, SK2, SK3) (Bond et al., 2005), and the K^+ channels underlying the M-current (KCNQ, Kv7.1-7.5) (Brown and Passmore, 2009), which mediate the fast afterhyperpolarization (AHP), the intermediate AHP/slow AHP, respectively (Andrade et al., 2012)

BK channels are gated by both voltage and cytoplasmic calcium and sculpt action potential firing in CNS neurons (Blatz and Magleby, 1987; Marty, 1989; Sah P., 1996; Storm, 1990). Indeed, BK channels have been shown to mediate rapid spike repolarization—*i.e*., the fast AHP in hippocampal CA1 pyramidal neurons (Lancaster and Nicoll, 1987; Storm, 1987). Blockade of BK channels in CA1 neurons attenuates the initial discharge frequency in response to current injection, which is attributable to suppression of the BK channel-dependent rapid spike repolarization (Lancaster and Nicoll, 1987; Storm, 1987). Blockade of BK channels is thought to increase inactivation of the spike-generating transient Na^+ current and activate more of the slower K^+ currents, thereby enhancing refractoriness and reducing excitability during the immediate aftermath of the first action potential (Shao et al., 1999). Thus, BK channels facilitate high-frequency burst firing of CA1 neurons. Furthermore, extracellular field recordings confirmed that BK channels contribute to high-frequency burst firing in response to excitatory synaptic input to distal dendrites in CA1 neurons (Gu et al., 2007). Therefore, BK channels appear to play an important role for early high-frequency, rapidly adapting firing in hippocampal CA1 pyramidal neurons, thus promoting the type of bursting that is characteristic of these cells *in vivo* during behavior. Based on our *in vitro* electrophysiological recordings and computational modeling we see a similar physiological phenomenon in $Kiss1^{ARH}$ neurons (**Figure 8**). Not only does E2 increase the mRNA expression of *Kcnma1* (**Figure 8G**), but also the maximum BK (IbTx-sensitive) current by 3-fold, which would facilitate rapid repolarization during burst firing and promote glutamate release similar to hippocampal CA1 neurons.

In contrast to BK channel expression, E2 did not affect the mRNA expression of SK3 channel mRNA. SK channels underlie the apamin-sensitive component of the medium duration AHP and are responsible for repolarization following a burst of action potentials (Andrade et al., 2012; Bond et al., 2005). The activation of SK channels is voltage-independent, but SK channels have a higher affinity for Ca^{2+} than BK channels (Andrade et al., 2012). SK channels are tightly coupled (within 100 nm) to L-type Ca^{2+} channels, and BK channels (within 30 nm) are tightly coupled to N-type Ca^{2+} channels in hippocampal CA1 pyramidal neurons (Marrion and Tavalin, 1998). The determination of the proximity of SK and BK channels to HVA calcium channels in kisspeptin neurons will require cell-attached patch recordings. However, in $Kiss1^{ARH}$ neurons the SK channels may come into play during a short burst of action potentials but would become overwhelmed with the higher frequency synchronized, sustained firing as a result of NKB stimulation (Qiu J. et al., 2016). As discussed above what limits the synchronized firing of $Kiss1^{ARH}$ neurons is the activation of GIRK channels.

Finally, the calcium-activated slow AHP probably plays a critical role in the repolarization of $Kiss1^{ARH}$ after burst firing. The molecular identification of the channels mediating the slow AHP has long been an area of intense

investigation (Andrade et al., 2012; Vogalis et al., 2003). A critical feature of the slow AHP is that it activates very slowly (hundreds of milliseconds) long after the rise in cytoplasmic Ca^{2+} (Sah P. and Clements, 1999) so an intermediate Ca^{2+} signaling molecule has long been thought to be involved. Indeed, Tzingounis and colleagues (Tzingounis A.V. et al., 2007) have provided compelling evidence that the diffusible calcium sensor hippocalcin is the critical intermediate molecule involved in Ca^{2+} sensing. The slow AHP is abrogated in hippocalcin KO mice, and transfection of hippocalcin into cultured hippocampal neurons generates a pronounced slow AHP in response to a depolarizing stimulus (Tzingounis A.V. et al., 2007). Importantly, the slow AHP is activated by Ca^{2+} with an $EC_{50} \approx 300$ nM, which is well within the operational range of hippocalcin but well below that of calmodulin (Andrade et al., 2012). Finally, two seminal papers from Tzingounis and colleagues demonstrate that KCNQ 2, 3 channels are responsible for the slow AHP in hippocampal dentate neurons (Tzingounis A. V. and Nicoll, 2008), and KCNQ 5 channels are responsible for the slow AHP in CA3 neurons (Tzingounis A. V. et al., 2010). Moreover, the KCNQ channel blocker XE991 attenuates the slow AHP in CA3 neurons (Tzingounis A. V. and Nicoll, 2008). Based on these seminal findings we investigated the role of the KCNQ channels, which "classically" underlie the M-current in $Kiss1^{ARH}$. The M-current was first identified in $Kiss1^{ARH}$ neurons by Conde and Roepke (Conde and Roepke, 2019), and presently we found that *Kcnq2* mRNA is expressed in $Kiss1^{ARH}$ neurons and up-regulated by E2, which translated into a greater M-current in $Kiss1^{ARH}$ neurons (**Figure 9**). Incorporating the M-current into our computational model indeed supports our hypothesis that M-current, along with I_{SK} and I_{BK}, contributes to membrane repolarization after burst firing (**Figure 9G**). Importantly the slow AHP, as opposed to the fast AHP (BK) and medium AHP (SK) is highly regulated by multiple neurotransmitters (Andrade et al., 2012), which sets the stage for further modulation of the slow EPSP in $Kiss1^{ARH}$ neurons.

Importance of E2-driven physiological transitioning

Since the expression of the peptide neurotransmitters in $Kiss1^{ARH}$ neurons are down-regulated by E2, the $Kiss1^{ARH}$ neurons are believed to be under "inhibitory" control by E2 and are important for "negative-feedback" regulation of GnRH release (Lehman et al., 2013; Navarro V. M. et al., 2009; Smith et al., 2005) (Rance Naomi E. and Young, 1991) (Rance N.E., 2009). However, our past (Gottsch et al., 2011) and current findings document that these $Kiss1^{ARH}$ neurons express HVA and LVA calcium and HCN (pacemaker) channels and are excited by co-released glutamate from neighboring $Kiss1^{ARH}$ neurons, which indicates that these neurons have pacemaker electrophysiological properties similar to other CNS neurons (Bal and McCormick, 1993; Lüthi and McCormick, 1998). Additionally, in contrast to the neuropeptides, E2 increases *Slc17a6* (*Vglut2*) mRNA expression, in addition to mRNA for the voltage-activated calcium and HCN channels, and increases glutamate release onto $Kiss1^{AVPV/PeN}$ neurons (Qiu J. et al., 2018). Interestingly, *Slc17a6* mRNA expression in $Kiss1^{ARH}$ neurons and the probability of glutamate release are decreased along with the neuropeptides in intact versus castrated males (Nestor et al., 2016), which indicates a profound sex difference in the glutamate signaling by

Kiss1^{ARH} neurons (Nestor et al., 2016; Qiu J. et al., 2018). Obviously, in the male there is no preovulatory LH surge so there is no need for excitatory glutamatergic input to the few Kiss1^{AVPV} neurons in the male.

In females, conditional knockout of *Slc17a6* in Kiss1 neurons abrogates glutamate release from Kiss1^{ARH} neurons (Qiu J. et al., 2018). Kiss1$^{AVPV/PeN}$ neurons do not express *Slc17a6* and do not release glutamate. Within the Kiss1^{ARH} neurocircuitry the lack of glutamate transmission does not diminish the slow EPSP in ovariectomized females (Qiu J. et al., 2018). Indeed, a recent publication from the Herbison lab demonstrates that glutamate generates small "synchronizing" events that are dependent on the ionotropic receptors (Han et al., 2023), but the fast neurotransmitter is unable to support the sustained firing (*i.e.*, slow EPSP) that is necessary for peptide release and synchronization of the KNDy network. Rather, we postulate that glutamate neurotransmission is more important for excitation of Kiss1$^{AVPV/PeN}$ neurons and facilitating the GnRH (LH) surge with high circulating levels of E2 when peptide neurotransmitters are at a nadir and glutamate levels are high in female Kiss1^{ARH} neurons. Indeed, low frequency (5 Hz) optogenetic stimulation of Kiss1^{ARH} neurons, which only releases glutamate in E2-treated, ovariectomized females (Qiu J. et al., 2016), generates a surge-like increase in LH release during periods of optical stimulation (Lin et al., 2021; Voliotis et al., 2021). In a subsequent study optical stimulation of Kiss1^{ARH} neuron terminals in the AVPV at 20 Hz, a frequency commonly used for terminal stimulation *in vivo*, generated a similar surge of LH (Shen et al., 2022). Additionally, intra-AVPV infusion of glutamate antagonists, AP5+CNQX, completely blocked the LH surge induced by Kiss1^{ARH} terminal photostimulation in the AVPV (Shen et al., 2022). Therefore, there appears to be a clear role for glutamatergic transmission from the Kiss1^{ARH} to Kiss1$^{AVPV/PeN}$ neurons in amplifying the LH surge in the female mouse. Finally it is important to keep in mind that even in the presence of high physiological levels of E2, the mRNA expression of *Tac2* is many-fold higher than *Kiss1* (**Figure 10**), which is essential for NKB maintaining synchronous firing of Kiss1^{ARH} neurons, albeit at a lower frequency, across all physiological states (Qiu J. et al., 2016). Indeed, there is a progressive change from a strictly pulsatile pattern of GnRH in the hypophyseal portal circulation to one containing both pulsatile and non-pulsatile components during the development of the GnRH surge in the ewe (Evans, Dahl, Mauger, & Karsch, 1995; Evans, Dahl, Mauger, Padmanabhan, et al., 1995), and a pulsatile mode of LH secretion during the preovulatory LH surge is also evident in other species including humans (Rossmanith et al., 1990). Therefore, we believe that our cellular molecular and electrophysiological findings in combination with our computational modelling provide a foundation for understanding the complex role of Kiss1^{ARH} neurons in controlling fertility in the mammal. Finally, our model provides the first comprehensive biophysical description of the conductances underlying the neuronal activity of Kiss^{ARH} neurons, which can serve as a basis for future computational modelling of the Kiss^{ARH} neuronal network and its interactions with other brain regions involved in the complex regulation of mammalian female reproduction.

Methods and Materials

Animals. All the animal procedures described in this study were performed in accordance with institutional guidelines based on National Institutes of Health standards and approved by the Institutional Animal Care and Use Committee at Oregon Health and Science University (OHSU).

Mice. *Kiss1*^{Cre} transgenic female mice version 2 (Padilla et al., 2018) were selectively bred at OHSU. They also were crossed with heterozygous Ai32 mice (RRID:IMSR_JAX:024109, C57BL/6 background) which carry ChR2 (H134R)–EYFP gene in their Gt(ROSA)26Sor locus (Madisen et al., 2012). All animals were maintained under controlled temperature and photoperiod (lights on at 0600h and off at 1800h) and given free access to food (Lab Diets 5L0D) and water. Where specified, Kiss1^{Cre} mice received viral injections to express channelrhodopsin 2 (ChR2) in Kiss1^{ARH} neurons, fourteen to twenty- one days prior to each experiment as described (Qiu J. et al., 2016). Some of the females were ovariectomized seven days prior to an experiment. Each animal was injected on day 5 following OVX with 0.25 µg E2 or vehicle, followed on day 6 with 1.50 µg E2 or vehicle and used for experiments on day 7 (Bosch et al., 2013).

AAV delivery to Kiss1^{Cre} *mice*. Fourteen to twenty-one days prior to each experiment, the *Kiss1*^{Cre} mice (>60 d old) received bilateral ARH injections of a Cre-dependent adeno-associated viral (AAV; serotype 1) vector encoding mCherry (AAV1-Ef1α-DIO-mCherry) or AAV1 vectors designed to encode SaCas9 and single-guide RNAs (sgRNAs) (See the SaCas9 section for specifics on the sgRNA design). Using aseptic techniques, anesthetized female mice (1.5% isoflurane/O_2) received a medial skin incision to expose the surface of the skull. The glass pipette with a beveled tip (diameter = 45 µm) was filled with mineral oil, loaded with an aliquot of AAV using a Nanoject II (Drummond Scientific). ARH injection coordinates were anteroposterior (AP): −1.20 mm, mediolateral (ML): ± 0.30 mm, dorsoventral (DV): −5.80 mm (surface of brain z = 0.0 mm); 500 nl of the AAV (2.0×10^{12} particles/ ml) was injected (100 nl/min) into each position, and the pipette left in place for 10 min post-injection, then slowly retracted from the brain. The skin incision was closed using Vetbond (3M) and each mouse received analgesia (Rimadyl, 4-5 mg/kg, *s.c.*).

Generation of AAV1-FLEX-SaCas9-U6-sgTrpc5. The generation of AAV1-FLEX-SaCas9-U6-sg*Trpc5* viruses were done at the University of Washington using published methods (Gore et al., 2013; Hunker et al., 2020). The constructs of sgRNAs for *Trpc5* (AAV1-FLEX-SaCas9-U6sg*Trpc5*) were designed to target exon2 and exon7, respectively (**Figure 11A and B**). To achieve *Trpc5* mutagenesis in Kiss1^{ARH} neurons, Kiss1^{Cre} mice were co-injected with AAV1-DIO-mCherry, AAV1-FLEX-SaCas9-U6-sg*Trpc5*-exon2, and AAV1-FLEX-SaCas9-U6-sg*Trpc5*-exon7 at a ratio of 10%, 45%, and 45%, respectively. Control animals were co-injected with AAV1-FLEX-SaCas9-U6-sg*Rosa26* and AAV1-DIO-mCherry at a ratio of 90% and 10%, respectively. AAV1-DIO-mCherry was co-injected with Cas9 vectors to confirm the targeting of injections and visualize the infected Kiss1^{ARH} neurons. Each animal was used for experiments three weeks after the viral injection, with OVX performed one week prior to the experiments.

Visualized whole-cell patch recording. Electrophysiological and optogenetic studies were made in coronal brain slices (250 µm) containing the ARH from AAV1-EF1α-DIO- mCherry injected Kiss1Cre:GFP or Kiss1-Cre:EYFP::AI32 mice, which were vehicle-treated OVX, and E2-treated OVX females 10 weeks and older as previously described (Qiu J. et al., 2016; Qiu J. et al., 2018). Whole-cell patch recordings were performed in voltage-clamp and current-clamp as previously described (Qiu J. et al., 2018) using an Olympus BX51 W1 fixed stage scope out-fitted with epifluorescence and IR-DIC video microscopy. Patch pipettes (A-M Systems; 1.5 µm outer diameter borosilicate glass) were pulled on a Brown/Flaming puller (Sutter Instrument, model P-97) and filled with the following solution (unless otherwise specified): 128 mM potassium gluconate, 10 mM NaCl, 1 mM $MgCl_2$, 11 mM EGTA, 10 mM HEPES, 2 mM ATP, and 0.25 mM GTP adjusted to pH 7.3 with KOH; 295 mOsm. Pipette resistances ranged from 3.5–4 MΩ. In whole-cell configuration, access resistance was less than 30 MΩ; the access resistance was 80% compensated. The input resistance was calculated by measuring the slope of the I-V relationship curve between −70 and −50 mV. Standard whole-cell patch recording procedures and pharmacological testing were performed as previously described (Qiu J. et al., 2003; Qiu J. et al., 2014). Electrophysiological signals were digitized with a Digidata 1322A (Axon Instruments) and the data were analyzed using p-Clamp software (Molecular Devices, Foster City, CA). The liquid junction potential was corrected for all data analysis.

For optogenetic stimulation, a light-induced response was evoked using a light-emitting diode (LED) 470 nm blue light source controlled by a variable 2A driver (ThorLabs, Newton, NJ) with the light path directly delivered through an Olympus 40x water-immersion lens. For high-frequency (20 Hz) stimulation the length of stimulation was 10 seconds (light intensity 0.9 mW and pulse duration, 10 ms) (Qiu J. et al., 2016).

For studying the firing pattern of $Kiss1^{ARH}$ neurons from OVX and E2-treated OVX mice, the electrodes were filled with an internal solution consisting of the following (in mM): 120 $KMeSO_4$, 5 Na_2 phosphocreatine, 10 KCl, 2 $MgSO_4$, 10 HEPES, 4 K_2ATP, and 0.25 GTP adjusted to pH 7.3 with KOH; 290 mOsm. The bath solution as described (Ashhad and Feldman, 2020) consisted of (in mM): 124 NaCl, 3.5 KCl, 25 $NaHCO_3$, 0.5 NaH_2PO_4 and 30 D-glucose,1 $MgSO_4$, 1.5 $CaCl_2$, gassed with 95% O_2 /5% CO_2 (pH 7.4, 310 mOsm).

For studying the activation/inactivation characteristics of the Ca^{2+} current, the electrodes were filled with an internal solution as described (Qiu J. et al., 2003) consisting of the following (in mM): 100 Cs^+ gluconate, 20 TEA-Cl, 10 NaCl, 1 $MgCl_2$, 10 HEPES, 11 EGTA, 1 ATP, 0.25 GTP, the pH was adjusted to 7.3 with CsOH at 300 mOsm. The bath solution as described (Zhang X. B. and Spergel, 2012) consisted of (in mM) 117.5 NaCl, 25 $NaHCO_3$, 1.25 NaH_2PO_4, 10 TEA-Cl, 2 $CaCl_2$, 1 $MgCl_2$, 20 sucrose and 5 glucose, gassed with 95% O_2 /5% CO_2 (pH 7.4, 309 mOsm) and supplemented with 1 µM TTX, 10 µM CNQX, 50 µM AP5 and 100 µM picrotoxin. The effects of estrogen treatment on the peak current, peak current density, and activation/inactivation characteristics of calcium current were measured. Activation curves were fitted by the Boltzmann equation: $I/I_{max}=1/\{1+\exp[V_{1/2}-Vs)/k]\}$, where I is the peak current at the step potential Vs, Imax is the peak current

amplitude, $V_{1/2}$ is the step potential yielding half-maximum current, and k is the slope factor. Inactivation curves were fit with the Boltzmann equation: $I/I_{max} = 1 - 1/ \{1 + \exp [(V_H - V_{1/2})/k]\}$, where I is the peak current at the step potential V_H, I_{max} is the peak current amplitude, $V_{1/2}$ is the step potential at which half the current is inactivated, and k is the slope factor.

To record M-currents, pipettes were filled with an internal solution consisting of 10 mM NaCl, 128 mM K-gluconate, 1 mM MgCl, 10 mM HEPES, 1 mM ATP, 1.1 mM EGTA, and 0.25 mM GTP (pH 7.3; 290 mOsm). During voltage-clamp, we employed a standard deactivation protocol (Conde and Roepke, 2019; Roepke et al., 2011) to measure potassium currents. This involved 500-ms voltage steps ranging from –30 to –75 mV in 5-mV increments, following a 300-millisecond prepulse to –20 mV. The amplitude of the M-current relaxation or deactivation was quantified as the difference between the initial (<10 ms) and sustained current (>475 ms) of the current trace.

The bath solution for whole-cell recording of BK, SK and M currents was aCSF supplemented with 1 μM TTX, 10 μM CNQX, 50 μM AP5 and 100 μM picrotoxin.

Electrophysiological solutions/drugs. A standard artificial cerebrospinal fluid (aCSF) was used (Qiu J. et al., 2003; Qiu J. et al., 2010). All drugs were purchased from Tocris Bioscience unless otherwise specified. 1 mM TTX (Alomone Labs), 50 mM DL-2-Amino-5-phosphonopentanoic acid sodium salt (AP5), 10 mM 6-Cyano-7-nitroquinoxaline-2,3-dione disodium (CNQX), 100 mM picrotoxin, 10 mM Nifedipine (Sigma), 2 mM ω-conotoxin GVIA (ConoGVIA; Alomone Labs), 0.5 mM ω-conotoxin MVIIC (ConoMVIIC; Alomone Labs, 50 μM ω-agatoxin IVA (AgaIVA; Alomone Labs), 50 μM SNX-482 (Alomone Labs), 10 mM TTA-P2 (TTAP2; Alomone Labs), 200 mM $CdCl_2$ (Cd^{2+}; Sigma), 40 mM XE991 (Alomone Labs), 100 μM Iberiotoxin (Alomone Labs), 500 μM Apamin (Alomone Labs), 100 mM glutamic acid and 1 mM senktide. Stocks (1000×) were prepared in dimethylsulfoxide DMSO (picrotoxin, TTA-P2 and senktide) or water (TTX, AP5, CNQX, ConoGVIA, ConoMVIIC, AgaIVA, SNX-482, $CdCl_2$ and glutamic acid) and stored at −20°C. Aliquots of the stock solutions were stored as appropriate until needed.

Cell harvesting of dispersed Kiss1^{Cre} neurons and real-time quantitative PCR (qPCR). Cell harvesting and qPCR was conducted as previously described (Bosch et al., 2013). The ARH was microdissected from basal hypothalamic coronal slices obtained from female Kiss1^{Cre} version 2 mice (Padilla et al., 2018) (n = 4-6 animals/group). The dispersed cells were visualized, patched, and then harvested (10 cells/tube) as described previously (Bosch et al., 2013). Briefly, ARH tissue was incubated in papain (7 mg/ml in oxygenated aCSF) for 50 min at 37° C then washed 4 times in low Ca^{2+} aCSF and two times in aCSF. For cell dispersion, Pasteur pipettes were flame polished to decreasing tip sizes and gentle trituration used to disperse the neurons onto a glass bottom dish. The plated cells were bathed in oxygenated aCSF using a peristaltic pump to keep the cells viable and clear of debris. Healthy cells with processes and a smooth cell membrane were harvested. Pipettes (World Precision Instruments; 1.5 μm outer diameter borosilicate glass) were pulled on a Brown/Flaming puller

(Sutter Instrument, model P-87) to a 10 µm diameter tip. The cells were harvested using the XenoWorks Microinjector System (Sutter Instruments, Navato, CA) which provides negative pressure in the pipette and fine control to draw the cell up into the pipette. Cell pools were harvested and stored at -80°C. All cell pools were DNAse-treated using DNase1. cDNA synthesis was performed as previously described (Bosch et al., 2013).

Primers for the genes that encode for low and high voltage-gated calcium channels, TRPC5, Vglut2, large conductance calcium-activated K^+ (BKα) channels, small conductance calcium-activated K^+ (SK3) channels and GAPDH were designed using Clone Manager software (Sci Ed Software) to cross at least one intron-exon boundary and optimized as previously described using Power Sybr Green method (Bosch et al., 2013). Real-time qPCR controls included neuronal pools without reverse transcriptase (-RT), hypothalamic RNA with RT (+) and without RT (-), as well as water blanks. Standard curves using ARH cDNA were utilized to determine the real-time PCR efficiency ($E = 10^{(-1/m)} - 1$) (Biosystems, 2006; Pfaffl, 2001). Only primers resulting in efficiencies of 90-100% were used for analysis. Primer sequences, qPCR parameters and efficiency calculations are provided in Table 1.

mRNA expression analysis. qPCR was performed on a Quantstudio 7 Flex Real-Time PCR System (Applied Biosystems) using Power SYBR Green PCR Master Mix (Applied Biosystems) according to established protocols (Bosch et al., 2013). The comparative $\Delta\Delta C_T$ method (Livak and Schmittgen, 2001; Pfaffl, 2001; Schmittgen and Livak, 2008) was used to determine values from duplicate samples of 4 µl for the target genes and 2 µl for the reference gene *GAPDH* in a 20 µl reaction volume containing 1x Power SYBR Green PCR Master Mix and 0.5 µM forward and reverse primers. Three to six 10-cell pools per animal were analyzed from 4-6 animals per group. The relative linear quantity was determined using the $2^{-\Delta\Delta CT}$ equation (Livak and Schmittgen, 2001; Pfaffl, 2001; Schmittgen and Livak, 2008). Relative mRNA expression level of target genes in $Kiss1^{Cre}$ neurons was obtained by comparing OVX Oil-treated controls to OVX E2-treated animals. The mean Δ CT for the target genes from the OVX Oil-treated control samples was used as the calibrator. The data were expressed as *n*-fold change in gene expression normalized to the reference gene *GAPDH* and relative to the calibrator.

Experimental design and Statistical analysis. For the whole-cell patch recording, pharmacological experiments, only one cell was recorded per slice. Two to three slices were analyzed from each $Kiss1^{Cre}$ mouse, with at least 3-5 mice contributing to each group. For cell harvesting of dispersed $Kiss1^{Cre}$-YFP neurons and qPCR measurements, 10 cells per pool and 3-6 pools from each animal were used, unless otherwise specified. Statistical comparisons between two groups were performed using an unpaired two-tailed Student's t-test. Comparisons between more than two groups were performed using the repeated measures, multifactorial ANOVA. If a significant interaction was encountered, we then moved to the one-way ANOVA, followed by the multiple range tests as specified in the appropriate figure legends. All data were analyzed

using GraphPad Prism version 6. All data are presented as mean ± standard error of the mean (SEM). Differences were considered statistically significant if the probability of error was less than 5%.

Mathematical model and simulation of neuronal behavior. A mathematical model of the Kiss1^{ARH} neuron was developed and calibrated based on our physiological findings. Here, we employed the Hodgkin-Huxley modelling approach (Hodgkin and Huxley, 1952). Accordingly, the equation describing the membrane potential V_m of the Kiss1^{ARH} neuron is given by

$$C_m \frac{dV_m}{dt} = -I,$$

where C_m is the membrane capacitance and I is the sum of 12 ionic currents:

$$I = I_{NaT} + I_{NaP} + I_A + I_{BK} + I_h + I_{SK} + I_M + I_T + I_{Ca} + I_{TRPC5} + I_{GRIK} + I_{leak}$$

I_{NaT} and I_{NaP} are the transient and persistent sodium currents, respectively; I_A represents the A current; I_M represents the M current; I_{SK} and I_{BK} are the potassium currents through the SK and BK channels respectively; I_h the HCN current; I_T the T-type calcium current; I_{Ca} represents other calcium currents (L-, N-, P/Q-, and R-type); I_{TRPC5} represents Calcium current throught the TRPC5 channel; I_{GIRK} potassium current through the GIRK channels. Finally, I_{leak} represents the contribution of leak currents. We use the Hodgkin-Huxley formalism to model current dynamics and their dependence on the membrane potential. A complete specification of all currents along with the complete table of model parameters can be found in the supplementary material. Model simulations were conducted in Matlab using the built-in numerical solver (ode45; based on an explicit Runge-Kutta (4, 5) formula). The Matlab code is available at https://git.exeter.ac.uk/mv286/kiss1-arcuate-neuron-model.

Acknowledgements

Funding

All electrophysiology and molecular biological studies were funded by the National Institutes of Health Grant R01-DK68098 (OKR and MJK, multi-PI). The generation of the *sgRNA's* was funded by National Institutes of Health Grants P30-MH048736 and R01104450 (LSZ). The computational modeling was funded by the BBSRC via grant BB/W0058831/1 (KTA and MV) and the EPSRC via grant EP/T017856/1 (KTA). The BBSRC also provided an International Partnership Award, BB/3019978/1, to facilitate collaboration between the UK partners (KOB, XFLi, KTA and MV) and the USA partners (MJK, OKR, JQ and MAB).

Author contributions

JQ designed, performed and analyzed the electrophysiological experiments and did the viral injections; MV performed the computational modeling and wrote the code; MAB designed, performed and analyzed the single cell harvesting and qPCR experiments; LSZ designed the *sgRNAs* against *TRPC5;* KTA provided resources for modeling; MJK and OKR conceived and designed the study, provided laboratory space and resources to conduct the experiments and wrote the manuscript with input from all the contributing authors.

Author ORCIDs

Martin J. Kelly: htpp://orcid.org/0000-0002-8633-2510

Jian Qiu: http://orcid.org/0000-0002-4988-8587

Oline K. Rønnekleiv: http://orcid.org/0000-0003-1841-4386

References

Ambudkar IS, & Ong HL. 2007. Organization and function of TRPC channelsomes. *Pflügers Archiv: European Journal of Physiology* **455**: 187-200. DOI:10.1007/s00424-007-0252-0, PMID: 17486362.

Andrade R, Foehring R, & Tzingounis A. 2012. The calcium-activated slow AHP: cutting through the Gordian knot. *Frontiers in Cellular Neuroscience* **6**: 47. DOI:10.3389/fncel.2012.00047, PMID: 23112761.

Arboit A, Reboreda A, & Yoshida M. 2020. Involvement of TRPC4 and 5 Channels in Persistent Firing in Hippocampal CA1 Pyramidal Cells. *Cells* **9**: 365. DOI:10.3390/cells9020365, PMID: 32033274.

Ashhad S, & Feldman JL. 2020. Emergent elements of inspiratory rhythmogenesis: network synchronization and synchrony propagation. *Neuron* **106**: 482-497. e484.

Bal T, & McCormick DA. 1993. Mechanisms of oscillatory activity in guinea-pig nucleus reticularis thalami *in vitro*: a mammalian pacemaker. *The Journal of Physiology* **468**: 669-691. DOI:10.1113/jphysiol.1993.sp019794, PMID: 8254530.

Bengtson CP, Tozzi A, Bernardi G, & Mercuri NB. 2004. Transient receptor potential-like channels mediate metabotropic glutamate receptor EPSCs in rat dopamine neurones. *The Journal of Physiology* **555**: 323-330. DOI:10.1113/jphysiol.2003.060061, PMID: 14724196.

Berg AP, Sen N, & Bayliss DA. 2007. TrpC3/C7 and Slo2.1 are molecular targets for metabotropic glutamate receptor signaling in rat striatal cholinergic interneurons. *The Journal of Neuroscience* **27**: 8845-8856. DOI:10.1523/JNEUROSCI.0551-07.2007, PMID: 17699666.

Biosystems A. 2006. Amplification efficiency of TaqMan Gene Expression Assays. *Applied Biosystems Application Note TaqMan Gene Expression Assays* **127AP05-03**.

Birnbaumer L. 2009. The TRPC class of ion channels: a critical review of their roles in slow, sustained increases in intracellular Ca^{2+} concentrations. *Annual Review of Pharmacology and Toxicology* **49**: 395-426. DOI:10.1146/annurev.pharmtox.48.113006.094928, PMID: 19281310.

Blair NT, Kaczmarek JS, & Clapham DE. 2009. Intracellular calcium strongly potentiates agonist-activated TRPC5 channels. *The Journal of General Physiology* **133**: 525-546. DOI:10.1085/jgp.200810153, PMID: 19398778.

Blatz AL, & Magleby KL. 1987. Calcium-activated potassium channels. *Trends in Neurosciences* **10**: 463-467.

Blum T, Moreno-Pérez A, Pyrski M, Bufe B, Arifovic A, Weissgerber P, Freichel M, Zufall F, & Leinders-Zufall T. 2019. Trpc5 deficiency causes hypoprolactinemia and altered function of oscillatory dopamine neurons in the arcuate nucleus. *Proceedings of the National Academy of Sciences* **116**: 15236-15243. DOI:10.1073/pnas.1905705116, PMID: 31285329.

Bond CT, Herson PS, Strassmaier T, Hammond R, Stackman R, Maylie J, & Adelman JP. 2004. Small conductance Ca^{2+}-activated K^{+} channel knock-out mice reveal the identity of calcium-dependent afterhyperpolarization currents. *The Journal of Neuroscience* **24**: 5301-5306. DOI:10.1523/JNEUROSCI.0182-04.2004, PMID: 15190101.

Bond CT, Maylie J, & Adelman JP. 1999. Small-conductance calcium-activated potassium channels. *Annals of the New York Academy of Sciences* **868**: 370-378. PMID: 10414306.

Bond CT, Maylie J, & Adelman JP. 2005. SK channels in excitability, pacemaking and synaptic integration. *Current Opinion in Neurobiology* **15**: 305-311. DOI:10.1016/j.conb.2005.05.001, PMID: 15922588.

Bosch MA, Kelly MJ, & Rønnekleiv OK. 2002. Distribution, neuronal co-localization and 17β-E2 modulation of small conductance calcium-activated K^+ channel (SK3) mRNA in the guinea pig brain. *Endocrinology* **143**: 1097-1107.

Bosch MA, Tonsfeldt KJ, & Rønnekleiv OK. 2013. mRNA expression of ion channels in GnRH neurons: subtype-specific regulation by 17β-Estradiol. *Molecular and Cellular Endocrinology* **367**: 85-97. DOI:10.1016/j.mce.2012.12.021, PMID: 23305677.

Brereton MF, Wareing M, Jones RL, & Greenwood SL. 2013. Characterisation of K+ Channels in Human Fetoplacental Vascular Smooth Muscle Cells. *PLOS One* **8**: e57451. DOI:10.1371/journal.pone.0057451,

Brown DA, & Passmore GM. 2009. Neural KCNQ (Kv7) channels. *British Journal of Pharmacology* **156**: 1185-1195. DOI:10.1111/j.1476-5381.2009.00111.x, PMID: 19298256.

Clapham DE. 2003. TRP channels as cellular sensors. *Nature* **426**: 517-524. DOI:10.1038/nature02196, PMID: 14654832.

Conde K, & Roepke T. 2019. 17β-estradiol increases arcuate KNDy neuronal sensitivity to ghrelin inhibition of the M-current in female mice. *Neuroendocrinology*: 10.1159/000503146. DOI:10.1159/000503146, PMID: 31484184.

d'Anglemont de Tassigny X, Fagg LA, Carlton MB, & Colledge WH. 2008. Kisspeptin can stimulate gonadotropin-releasing hormone (GnRH) release by a direct action at GnRH nerve terminals. *Endocrinology* **149**: 3926-3932.

De Roux N, Genin E, Carel J-C, Matsuda F, Chaussain J-L, & Milgrom E. 2003. Hypogonadotropic hypogonadism due to loss of function of the KiSS 1-derived peptide receptor GPR54. *Proceedings of the National Academy of Sciences of the United States of America* **100**: 10972-10976. DOI:10.1073/pnas.1834399100, PMID: 12944565.

Erickson KR, Rønnekleiv OK, & Kelly MJ. 1993a. Electrophysiology of guinea-pig supraoptic neurones: role of a hyperpolarization-activated cation current in phasic firing. *The Journal of Physiology* **460**: 407-425. PMID: 8487202.

Erickson KR, Rønnekleiv OK, & Kelly MJ. 1993b. Role of a T-type calcium current in supporting a depolarizing potential, damped oscillations, and phasic firing in vasopressinergic guinea pig supraoptic neurons. *Neuroendocrinology* **57**: 789-800. DOI:10.1159/000126438, PMID: 8413816.

Evans NP, Dahl GE, Mauger D, & Karsch FJ. 1995. Estradiol induces both qualitative and quantitative changes in the pattern of gonadotropin-releasing hormone secretion during the presurge period in the ewe. *Endocrinology* **136**: 1603-1609.

Evans NP, Dahl GE, Mauger DT, Padmanabhan V, Thrun LA, & Karsch FJ. 1995. Does estradiol induce the preovulatory gonadotropin-releasing hormone (GnRH) surge in the ewe by inducing a progressive change in the mode of operation of the GnRH neurosecretory system. *Endocrinology* **136**: 5511-5519.

Faber ES, Sedlak P, Vidovic M, & Sah P. 2006. Synaptic activation of transient receptor potential channels by metabotropic glutamate receptors in the lateral amygdala. *Neuroscience* **137**: 781-794. DOI:10.1016/j.neuroscience.2005.09.027, PMID: 16289832.

Goodman RL, Lehman MN, Smith JT, Coolen LM, de Oliveira CVR, Jafarzadehshirazi MR, Pereira A, Iqbal J, Caraty A, Ciofi P, & Clarke IJ. 2007. Kisspeptin neurons in the arcuate nucleus of the ewe express both dynorphin A and neurokinin B. *Endocrinology* **148**: 5752-5760. DOI:10.1210/en.2007-0961, PMID: 17823266.

Gore BB, Soden ME, & Zweifel LS. 2013. Manipulating gene expression in projection-specific neuronal populations using combinatorial viral approaches. *Current Protocols in Neuroscience* **65**: 1-20. DOI:10.1002/0471142301.ns0435s65, PMID: 25429312.

Gottsch ML, Popa SM, Lawhorn JK, Qiu J, Tonsfeldt KJ, Bosch MA, Kelly MJ, Rønnekleiv OK, Sanz E, McKnight GS, Clifton DK, Palmiter RD, & Steiner RA. 2011. Molecular properties of Kiss1 neurons in the arcuate nucleus of the mouse. *Endocrinology* **152**: 4298-4309. DOI:10.1210/en.2011-1521, PMID: 21933870.

Greene DL, Kang S, & Hoshi N. 2017. XE991 and linopirdine are state-dependent inhibitors for Kv7/KCNQ channels that favor activated single subunits. *Journal of Pharmacology and Experimental Therapeutics* **362**: 177-185. DOI:10.1124/jpet.117.241679, PMID: 28483800.

Gu N, Vervaeke K, & Storm JF. 2007. BK potassium channels facilitate high-frequency firing and cause early spike frequency adaptation in rat CA1 hippocampal pyramidal cells. *The Journal of Physiology* **580**: 859-882. DOI:https://doi.org/10.1113/jphysiol.2006.126367,

Han SY, Morris PG, Kim J-C, Guru S, Pardo-Navarro M, Yeo S-H, McQuillan HJ, & Herbison AE. 2023. Mechanism of kisspeptin neuron synchronization for pulsatile hormone secretion in male mice. *Cell Reports* **42**: 111914. DOI:https://doi.org/10.1016/j.celrep.2022.111914,

Hiraizumi Y, Nishimura I, Ishii H, Tanaka N, Takeshita T, Sakuma Y, & Kato M. 2008. Rat GnRH neurons exhibit large conductance voltage- and Ca^{2+}-Activated K^{+} (BK) currents and express BK channel mRNAs. *The Journal of Physiological Sciences* **58**: 21-29. DOI:10.2170/physiolsci.RP013207, PMID: 18177544.

Hodgkin AL, & Huxley AF. 1952. A quantitative description of membrane current and its application to conduction and excitation in nerve. *The Journal of Physiology* **117**: 500-544. PMID: 12991237.

Hunker AC, Soden ME, Krayushkina D, Heymann G, Awatramani R, & Zweifel LS. 2020. Conditional single vector CRISPR/SaCas9 viruses for efficient mutagenesis in the adult mouse nervous system. *Cell Reports* **30**: 4303-4316 e4306. DOI:10.1016/j.celrep.2020.02.092, PMID: 32209486.

Kato M, Ui-Tei K, Watanabe M, & Sakuma Y. 2003. Characterization of voltage-gated calcium currents in gonadotropin-releasing hormone neurons tagged with green fluorescent protein in rats. *Endocrinology* **144**: 5118-5125. DOI:10.1210/en.2003-0213, PMID: 12960038.

Kelly MJ, Qiu J, & Rønnekleiv OK. 2018. TRPCing around the hypothalamus. *Frontiers in Neuroendocrinology* **51**: 116-124. DOI:10.1016/j.yfrne.2018.05.004, PMID: 29859883.

Kelly MJ, & Rønnekleiv OK. 1994. Electrophysiological analysis of neuroendocrine neuronal activity in hypothalamic slices. In J. E. Levine (Ed.), *Methods in Neurosciences: Pulsatility in Neuroendocrine Systems* (1 ed., pp. 47-67). San Diego: Academic Press, Inc. (Reprinted from: In File).

Kotani M, Detheux M, Vandenbogaerde A, Communi D, Vanderwinden JM, Le Poul E, Brezillon S, Tyldesley R, Suarez-Huerta N, Vandeput F, Blanpain C, Schiffmann SN, Vassart G, & Parmentier M. 2001. The metastasis suppressor gene KiSS-1 encodes kisspeptins, the natural ligands of the orphan G protein-coupled receptor GPR54. *Journal of Biological Chemistry* **276**: 34631-34636. DOI:10.1074/jbc.M104847200, PMID: 11457843.

Kshatri AS, Gonzalez-Hernandez A, & Giraldez T. 2018. Physiological Roles and Therapeutic Potential of Ca2+ Activated Potassium Channels in the Nervous System. *Frontiers in Molecular Neuroscience* **11**. DOI:10.3389/fnmol.2018.00258,

Lancaster B, & Nicoll RA. 1987. Properties of two calcium-activated hyperpolarizations in rat hippocampal neurones. *The Journal of Physiology* **389**: 187-203. PMID: 2445972.

Lee S-C, Choi S, Lee T, Kim H-L, Chin H, & Shin H-S. 2002. Molecular basis of R-type calcium channels in central amygdala neurons of the mouse. *Proceedings of the National Academy of Sciences* **99**: 3276-3281. DOI:doi:10.1073/pnas.052697799,

Lehman MN, Hileman SM, & Goodman RL. 2013. Neuroanatomy of the kisspeptin signaling system in mammals: comparative and developmental aspects. *Advances in Experimental Medicine and Biology* **784**: 27-62. DOI:10.1007/978-1-4614-6199-9_3, PMID: 23550001.

Lehman MN, Merkley CM, Coolen LM, & Goodman RL. 2010. Anatomy of the kisspeptin neural network in mammals. *Brain Research* **1364**: 90-102. DOI:10.1016/j.brainres.2010.09.020, PMID: 20858464.

Lin XH, Lass G, Kong LS, Wang H, Li XF, Huang HF, & O'Byrne KT. 2021. Optogenetic Activation of Arcuate Kisspeptin Neurons Generates a Luteinizing Hormone Surge-Like Secretion in an Estradiol-Dependent Manner. *Front Endocrinol (Lausanne)* **12**: 775233. DOI:10.3389/fendo.2021.775233, PMID: 34795643.

Liu X, Yeo S-H, McQuillan HJ, Herde MK, Hessler S, Cheong I, Porteous R, & Herbison AE. 2021. Highly redundant neuropeptide volume co-transmission underlying episodic activation of the GnRH neuron dendron. *eLife* **10**: e62455. DOI:10.7554/eLife.62455,

Livak KJ, & Schmittgen TD. 2001. Analysis of relative gene expression data using real-time quantitative PCR and the $2^{-\Delta\Delta CT}$ method. *Methods* **25**: 402-408. DOI:10.1006/meth.2001.1262, PMID: 11846609.

Llinás RR. 1988. The intrinsic electrophysiological properties of mammalian neurons: insights into central nervous system function. *Science* **242**: 1654-1664.

Lüthi A, & McCormick DA. 1998. H-current: properties of a neuronal and network pacemaker. *Neuron* **21**: 9-12. DOI:10.1016/S0896-6273(00)80509-7, PMID: 9697847.

Lyons DJ, Hellysaz A, & Broberger C. 2012. Prolactin regulates tuberoinfundibular dopamine neuron discharge pattern: novel feedback control mechanisms in the lactotrophic axis. *The Journal of Neuroscience* **32**: 8074-8083. DOI:10.1523/JNEUROSCI.0129-12.2012, PMID: 22674282.

Lyons DJ, Horjales-Araujo E, & Broberger C. 2010. Synchronized network oscillations in rat tuberoinfundibular dopamine neurons: swith to tonic discharge by thyrotropin-releasing hormone. *Neuron* **65**: 217-229.

Madisen L, Mao T, Koch H, Zhuo JM, Berenyi A, Fujisawa S, Hsu YW, Garcia AJ, 3rd, Gu X, Zanella S, Kidney J, Gu H, Mao Y, Hooks BM, Boyden ES, Buzsaki G, Ramirez JM, Jones AR, Svoboda K, Han X, Turner EE, & Zeng H. 2012. A toolbox of Cre-dependent optogenetic transgenic mice for light-induced activation and silencing. *Nature Neuroscience* **15**: 793-802. DOI:10.1038/nn.3078, PMID: 22446880.

Marrion NV, & Tavalin SJ. 1998. Selective activation of Ca^{2+}-activated K^{+} channels by co-localize Ca^{2+} channels in hippocampal neurons. *Nature* **395**: 900-905.

Marty A. 1989. The physiological role of calcium-dependent channels. *Trends in Neurosciences* **12**: 420-424. PMID: 2479142.

McNally BA, Plante AE, & Meredith AL. 2020. Diurnal properties of voltage-gated Ca2+ currents in suprachiasmatic nucleus and roles in action potential firing. *The Journal of Physiology* **598**: 1775-1790. DOI:https://doi.org/10.1113/JP278327,

Mendonça PRF, Kyle V, Yeo SH, Colledge WH, & Robinson HPC. 2018. Kv4.2 channel activity controls intrinsic firing dynamics of arcuate kisspeptin neurons. *The Journal of Physiology* **596**: 885-899. DOI:10.1113/JP274474, PMID: 29214635.

Messager S, Chatzidaki EE, Ma D, Hendrick AG, Zahn D, Dixon J, Thresher RR, Malinge I, Lomet D, Carlton MB, Colledge WH, Caraty A, & Aparicio SA. 2005. Kisspeptin directly stimulates gonadotropin-releasing hormone release via G protein-coupled receptor 54. *Proceedings of the National Academy of Sciences of the United States of America* **102**: 1761-1766. DOI:10.1073/pnas.0409330102, PMID: 15665093.

Moenter SM, Caraty A, Lehman MN, & Karsch FJ. 1993. Characterization and regulation of pre-ovulatory secretion of gonadotrophin-releasing hormone. *Human Reproduction* **8 Suppl 2**: 51-56. PMID: 8276969.

Navarro VM, Gottsch ML, Chavkin C, Okamura H, Clifton DK, & Steiner RA. 2009. Regulation of gonadotropin-releasing hormone secretion by kisspeptin/dynorphin/neurokinin B neurons in the arcuate nucleus of the mouse. *The Journal of Neuroscience* **29**: 11859-11866. DOI:10.1523/JNEUROSCI.1569-09.2009, PMID: 19776272.

Navarro VM, Gottsch ML, Wu M, García-Galiano D, Hobbs SJ, Bosch MA, Pinilla L, Clifton DK, Dearth A, Rønnekleiv OK, Braun RE, Plamiter RD, Tena-Sempere M, Alreja M, & Steiner RA. 2011. Regulation of NKB pathways and their roles in the control of Kiss1 neurons in the arcuate nucleus of the male mouse. *Endocrinology* **152**: 4265-4275. DOI:10.1210/en.2011-1143, PMID: 21914775.

Nestor CC, Qiu J, Padilla SL, Zhang C, Bosch MA, Fan W, Aicher SA, Palmiter RD, Rønnekleiv OK, & Kelly MJ. 2016. Optogenetic stimulation of arcuate nucleus Kiss1 neurons reveals a steroid-dependent glutamatergic input to POMC and AgRP neurons in male mice. *Molecular Endocrinology* **30**: 630-644. DOI:10.1210/me.2016-1026, PMID: 27093227.

Nicoll RA. 1988. The coupling of neurotransmitter receptors to ion channels in the brain. *Science* **241**: 545-551. PMID: 2456612.

Niday Z, & Bean BP. 2021. BK Channel Regulation of Afterpotentials and Burst Firing in Cerebellar Purkinje Neurons. *The Journal of Neuroscience* **41**: 2854-2869. DOI:10.1523/jneurosci.0192-20.2021,

Nunemaker CS, DeFazio RA, & Moenter SM. 2003. Calcium current subtypes in GnRH neurons. *Biology of Reproduction* **69**: 1914-1922. DOI:10.1095/biolreprod.103.019265, PMID: 12904316.

O'Byrne KT, Thalabard JC, Grosser PM, Wilson RC, Williams CL, Chen MD, Ladendorf D, Hotchkiss J, & Knobil E. 1991. Radiotelemetric monitoring of hypothalamic gonadotropin-releasing hormone pulse generator activity throughout the menstrual cycle of the rhesus monkey. *Endocrinology* **129**: 1207-1214. DOI:10.1210/endo-129-3-1207, PMID: 1874166.

Padilla SL, Johnson CW, Barker FD, Patterson MA, & Palmiter RD. 2018. A neural circuit underlying the generation of hot flushes. *Cell Reports* **24**: 271-277. DOI:10.1016/j.celrep.2018.06.037, PMID: 29996088.

Perez-Reyes E. 2003. Molecular physiology of low-voltage-activated t-type calcium channels. *Physiological Reviews* **83**: 117-161. DOI:10.1152/physrev.00018.2002, PMID: 12506128.

Peters HC, Hu H, Pongs O, Storm JF, & Isbrandt D. 2005. Conditional transgenic suppression of M channels in mouse brain reveals functions in neuronal excitability, resonance and behavior. *Nature Neuroscience* **8**: 51-60. DOI:10.1038/nn1375, PMID: 15608631.

Pfaffl MW. 2001. A new mathematical model for relative quantification in real-time RT-PCR. *Nucleic Acids Research* **29**: e45. DOI:10.1093/nar/29.9.e45, PMID: 11328886.

Qiu J, Bosch MA, Tobias SC, Grandy DK, Scanlan TS, Rønnekleiv OK, & Kelly MJ. 2003. Rapid signaling of estrogen in hypothalamic neurons involves a novel G-protein-coupled estrogen receptor that activates protein kinase C. *The Journal of Neuroscience* **23**: 9529-9540. DOI:10.1523/JNEUROSCI.23-29-09529.2003, PMID: 14573532.

Qiu J, Fang Y, Rønnekleiv OK, & Kelly MJ. 2010. Leptin excites proopiomelanocortin neurons via activation of TRPC channels. *The Journal of Neuroscience* **30**: 1560-1565. DOI:10.1523/JNEUROSCI.4816-09.2010, PMID: 20107083.

Qiu J, Nestor CC, Zhang C, Padilla SL, Palmiter RD, Kelly MJ, & Rønnekleiv OK. 2016. High-frequency stimulation-induced peptide release synchronizes arcuate kisspeptin neurons and excited GnRH neurons. *eLife* **5**: e16246. DOI:10.7554/eLife.16246, PMID: 27549338.

Qiu J, Rivera HM, Bosch MA, Padilla SL, Stincic TL, Palmiter RD, Kelly MJ, & Rønnekleiv OK. 2018. Estrogenic-dependent glutamatergic neurotransmission from kisspeptin neurons governs feeding circuits in females. *eLife* **7**: e35656. DOI:10.7554/eLife.35656, PMID: 30079889.

Qiu J, Stincic TL, Bosch MA, Connors AM, Petrie SK, Rønnekleiv OK, & Kelly MJ. 2021. Deletion of Stim1 in hypothalamic arcuate nucleus Kiss1 neurons potentiates synchronous GCaMP activity and protects against diet-induced obesity. *J Neurosc* **41**: 9688-9701. DOI:https://doi.org/10.1523/JNEUROSCI.0622-21.2021,

Qiu J, Zhang C, Borgquist A, Nestor CC, Smith AW, Bosch MA, Ku S, Wagner EJ, Rønnekleiv OK, & Kelly MJ. 2014. Insulin excites anorexigenic proopiomelanocortin neurons via activation of canonical transient receptor potential channels. *Cell Metabolism* **19**: 682-693. DOI:10.1016/j.cmet.2014.03.004, PMID: 24703699.

Rance NE. 2009. Menopause and the human hypothalamus: Evidence for the role of kisspeptin/neurokinin B neurons in the regulation of esstrogen negative feedback. *Peptides* **30**: 111-122.

Rance NE, & Young WS, III. 1991. Hypertrophy and Increased Gene Expression of Neurons Containing Neurokinin-B and Substance-P Messenger Ribonucleic Acids in the Hypothalami of Postmenopausal Women*. *Endocrinology* **128**: 2239-2247. DOI:10.1210/endo-128-5-2239,

Roepke TA, Qiu J, Smith AW, Rønnekleiv OK, & Kelly MJ. 2011. Fasting and 17β-estradiol differentially modulate the M-current in neuropeptide Y neurons. *The Journal of Neuroscience* **17**: 11825-11835. DOI:10.1523/JNEUROSCI.1395-11.2011, PMID: 21849543.

Rønnekleiv OK, Qiu J, & Kelly MJ. 2022. Hypothalamic Kisspeptin Neurons and the Control of Homeostasis. *Endocrinology* **163**: 1-11. DOI:10.1210/endocr/bqab253,

Rossmanith WG, Liu CH, Laughlin GA, Mortola JF, Suh BY, & Yen SSC. 1990. Relative changes in LH pulsatility during the menstrual cycle: Using data from hypogonadal women as a reference point. *Clinical Endocrinology* **32**: 647-660. DOI:https://doi.org/10.1111/j.1365-2265.1990.tb00909.x,

Sah P. 1996. Ca^{2+}-activated K^+ currents in neurones: Types, physiological roles and modulation. *Trends in Neurosciences* **19**: 150-154.

Sah P, & Clements JD. 1999. Photolytic manipulation of $[Ca^{2+}]_i$ reveals slow kinetics of potassium channels underlying the afterhyperpolarization in hippocampal pyramidal neurons. *The Journal of Neuroscience* **19**: 3657-3664. PMID: 10233997.

Sah P, & Louise Faber ES. 2002. Channels underlying neuronal calcium-activated potassium currents. *Progress in Neurobiology* **66**: 345-353. DOI:https://doi.org/10.1016/S0301-0082(02)00004-7,

Schmittgen TD, & Livak KJ. 2008. Analyzing real-time PCR data by the comparative C_T method. *Nature Protocols* **3**: 1101-1108.

Seminara SB, Messager S, Chatzidaki EE, Thresher RR, Acierno JS, Shagoury JK, Bo-Abbas Y, Kuohung W, Schwinof KM, Hendrick AG, Zahn D, Dixon J, Kaiser UB, Slaugenhaupt SA, Gusella JF, O'Rahilly S, Carlton MBL, Crowley WF, Aparicio SAJR, & Colledge WH. 2003. The GPR54 gene as a regulator of puberty. *The New England Journal of Medicine* **349**: 1614-1627. DOI:10.1056/NEJMoa035322, PMID: 14573733.

Shahab M, Mastronardi C, Seminara SB, Crowley WF, Ojeda SR, & Plant TM. 2005. Increased hypothalamic GPR54 signaling: a potential mechanism for initiation of puberty in primates. *Proceedings of the National Academy of Sciences of the United States of America* **102**: 2129-2134. DOI:10.1073/pnas.0409822102, PMID: 15684075.

Shao LR, Halvorsrud R, Borg-Graham L, & Storm JF. 1999. The role of BK-type Ca2+-dependent K+ channels in spike broadening during repetitive firing in rat hippocampal pyramidal cells. *The Journal of Physiology* **521 Pt 1**: 135-146. PMID: 10562340.

Shen X, Liu Y, Li XF, Long H, Wang L, Lyu Q, Kuang Y, & O'Byrne KT. 2022. Optogenetic stimulation of Kiss1ARC terminals in the AVPV induces surge-like luteinizing hormone secretion via glutamate release in mice. *Frontiers in Endocrinology* **13**. DOI:10.3389/fendo.2022.1036235,

Smith JT, Cunningham MJ, Rissman EF, Clifton DK, & Steiner RA. 2005. Regulation of *Kiss1* gene expression in the brain of the female mouse. *Endocrinology* **146**: 3686-3692. DOI:10.1210/en.2005-0488, PMID: 15919741.

Spergel DJ. 2007. Calcium and small-conductance calcium-activated potassium channels in gonadotropin-releasing hormone neurons before, during, and after puberty. *Endocrinology* **148**: 2383-2390.

Stincic TL, Bosch MA, Hunker AC, Juarez B, Connors AM, Zweifel LS, Rønnekleiv OK, & Kelly MJ. 2021. CRISPR knockdown of Kcnq3 attenuates the M current and increases excitability of NPY/AgRP neurons to alter energy balance. *Molecular Metabolism*: 101218. DOI:https://doi.org/10.1016/j.molmet.2021.101218,

Storm JF. 1987. Action potential repolarization and a fast after-hyperpolarization in rat hippocampal pyramidal cells. *The Journal of Physiology* **385**: 733-759. PMID: 2443676.

Storm JF. 1990. Potassium currents in hippocampal pyramidal cells. *Progress in Brain Research* **83**: 161-187. PMID: 2203097.

Tian J-b, Yang J, Joslin WC, Flockerzi V, Prescott SA, Birnbaumer L, & Zhu MX. 2022. TRPC4 and GIRK channels underlie neuronal coding of firing patterns that reflect $G_{q/11}$–$G_{i/o}$ coincidence signals of variable strengths. *Proceedings of the National Academy of Sciences* **119**: e2120870119. DOI:doi:10.1073/pnas.2120870119,

Tozzi A, Bengtson CP, Longone P, Carignani C, Fusco FR, Bernardi G, & Mercuri NB. 2003. Involvement of transient receptor potential-like channels in responses to mGluR-I activation in midbrain dopamine neurons. *European Journal of Neuroscience* **18**: 2133-2145. DOI:10.1046/j.1460-9568.2003.02936.x, PMID: 14622174.

Tsien RW, Hess P, McCleskey EW, & Rosenberg RL. 1987. Calcium channels: mechanisms of selectivity, permeation, and block. *Annual Review of Biophysics and Biophysical Chemistry* **16**: 265-290. DOI:10.1146/annurev.bb.16.060187.001405, PMID: 2439098.

Tzingounis AV, Heidenreich M, Kharkovets T, Spitzmaul G, Jensen HS, Nicoll RA, & Jentsch TJ. 2010. The KCNQ5 potassium channel mediates a component of the afterhyperpolarization current in mouse hippocampus. *Proceedings of the National Academy of Sciences of the United States of America* **107**: 10232-10237. DOI:10.1073/pnas.1004644107, PMID: 20534576.

Tzingounis AV, Kobayashi M, Takamatsu K, & Nicoll RA. 2007. Hippocalcin gates the calcium activation of the slow afterhyperpolarization in hippocampal pyramidal cellls. *Neuron* **53**: 487-493.

Tzingounis AV, & Nicoll RA. 2008. Contribution of KCNQ2 and KCNQ3 to the medium and slow afterhyperpolarization currents. *Proceedings of the National Academy of Sciences of the United States of America* **105**: 19974-19979. DOI:10.1073/pnas.0810535105, PMID: 19060215.

Venkatachalam K, & Montell C. 2007. TRP channels. *Annual Review of Biochemistry* **76**: 387-417. DOI:10.1146/annurev.biochem.75.103004.142819, PMID: 17579562.

Vogalis F, Storm JF, & Lancaster B. 2003. SK channels and the varieties of slow after-hyperpolarizations in neurons. *European Journal of Neuroscience* **18**: 3155-3166. PMID: 14686890.

Voliotis M, Li XF, De Burgh RA, Lass G, Ivanova D, McIntyre C, O'Byrne K, & Tsaneva-Atanasova K. 2021. Modulation of pulsatile GnRH dynamics across the ovarian cycle via changes in the network excitability and basal activity of the arcuate kisspeptin network. *eLife* **10**: e71252. DOI:10.7554/eLife.71252,

Wakabayashi Y, Nakada T, Murata K, Ohkura S, Mogi K, Navarro VM, Clifton DK, Mori Y, Tsukamura H, Maeda K-I, Steiner RA, & Okamura H. 2010. Neurokinin B and dynorphin A in kisspeptin neurons of the arcuate nucleus participate in generation of periodic oscillation of neural activity driving pulsatile gonadotropin-releasing hormone secretion in the goat. *The Journal of Neuroscience* **30**: 3124-3132. DOI:10.1523/JNEUROSCI.5848-09.2010, PMID: 20181609.

Whorton MR, & MacKinnon R. 2011. Crystal structure of the mammalian GIRK2 K+ channel and gating regulation by G proteins, PIP2, and sodium. *Cell* **147**: 199-208. DOI:10.1016/j.cell.2011.07.046, PMID: 21962516.

Zagotta WN, & Siegelbaum SA. 1996. Structure and function of cyclic nucleotide-gated channels. *Annual Review of Neuroscience* **19**: 235-263. DOI:10.1146/annurev.ne.19.030196.001315, PMID: 8833443.

Zhang C, Bosch MA, Rick EA, Kelly MJ, & Rønnekleiv OK. 2009. 17β-estradiol regulation of T-type calcium channels in gonadotropin-releasing hormone neurons. *The Journal of Neuroscience* **29**: 10552-10562. DOI:10.1523/JNEUROSCI.2962-09.2009, PMID: 19710308.

Zhang C, Rønnekleiv OK, & Kelly MJ. 2013. Kisspeptin inhibits a slow afterhyperpolarization current via protein kinase C and reduces spike frequency adaptation in GnRH neurons. *American Journal of Physiology: Endocrinology and Metabolism* **304**: E1237-1244. DOI:10.1152/ajpendo.00058.2013, PMID: 23548613.

Zhang XB, & Spergel DJ. 2012. Kisspeptin inhibits high-voltage activated Ca^{2+} channels in GnRH neurons via multiple Ca^{2+} influx and release pathways. *Neuroendocrinology* **96**: 68-80. DOI:10.1159/000335985, PMID: 22343183.

Zhang Z, Reboreda A, Alonso A, Barker PA, & Séguéla P. 2011. TRPC channels underlie cholinergic plateau potentials and persistent activity in entorhinal cortex. *Hippocampus* **21**: 386-397. DOI:https://doi.org/10.1002/hipo.20755,

Zheng Y, Liu H, Chen Y, Dong S, Wang F, Wang S, Li G-L, Shu Y, & Xu F. 2022. Structural insights into the lipid and ligand regulation of a human neuronal KCNQ channel. *Neuron* **110**: 237-247.e234. DOI:https://doi.org/10.1016/j.neuron.2021.10.029,

Zylberberg J, & Strowbridge BW. 2017. Mechanisms of Persistent Activity in Cortical Circuits: Possible Neural Substrates for Working Memory. *Annual Review of Neuroscience* **40**: 603-627. DOI:10.1146/annurev-neuro-070815-014006, PMID: 28772102.

Table 1. Primer Table

Gene Name (encodes for)	Accession Number	Primer Location (bp)	Product Length (bp)	Annealing Temp (°C)	Efficiency Slope	r^2	%
Cacna1c (Cav 1.2 L-type)	NM_009781	1331-1348 1390-1407	77	60	-3.478	0.989	94
Cacna1a (Cav 2.1 P/Q-type)	NM_007578	6035-6054 6090-6109	75	60	-3.498	0.980	93
Cacna1b (Cav 2.2 (N-type)	NM_001042528	5405-5426 5467-5488	84	60	-3.483	0.992	94
Cacna1e (Cav 2.3 R-type)	NM_009782	530-549 617-636	107	60	-3.441	0.983	95
Cacna1g (Cav 3.1 T-type)	NM_009783	5004-5025 5060-5083	80	60	-3.372	0.968	98
Hcn1 (HCN1)	NM_010408	1527-1546 1641-1662	136	60	-3.253	0.958	100
Kcnd2 (KCND2)	NM_019697	2135-2156 2217-2238	104	60	-3.312	0.972	100
Kcnn3 (SK3)	NM_080466	1259-1277 1352-1370	112	60	-3.369	0.952	98

Kcnma1 (BK)	NM_001253358	2745-2762 2833-2852	108	60	-3.338	0.971	99
Kcnb1 (KCNB1)	NM_008420	734-751 835-852	119	60	-3.375	0.983	98
Kcnq2 (KCNQ2)	NM_010611	1079-1098 1151-1170	92	60	-3.367	0.978	98
Tac2 (NKB)	NM_009312	368-389 490-511	144	60	-3.440	0.989	95
Slc17a6 (vGluT2)	NM_080853	1275-1296 1371-1390	116	60	-3.374	0.997	98
Trpc5 (TRPC5)[a]	NM_009428	734-753 832-851	118	60	-3.161	0.952	100
Trpc5 (TRPC5)[b]	NM_009428	616-637 772-792	177	60	-3.407	0.987	97
Trpc5 (TRPC5)[b]	NM_009428	2083-2100 2162-2179	97	60	-3.255	0.963	100
Kcnj6 (GIRK2)	NM_001025584	488-507 592-609	122	60	-3.368	0.919	98
Gapdh (GAPDH)	NM_008084	689-706 764-781	93	60	-3.352	0.998	99

[a] *Trpc5* primers figure 10E. [b] *Trpc5* primers flanking sgRNA and PAM sites in mutagenesis figure 11D.

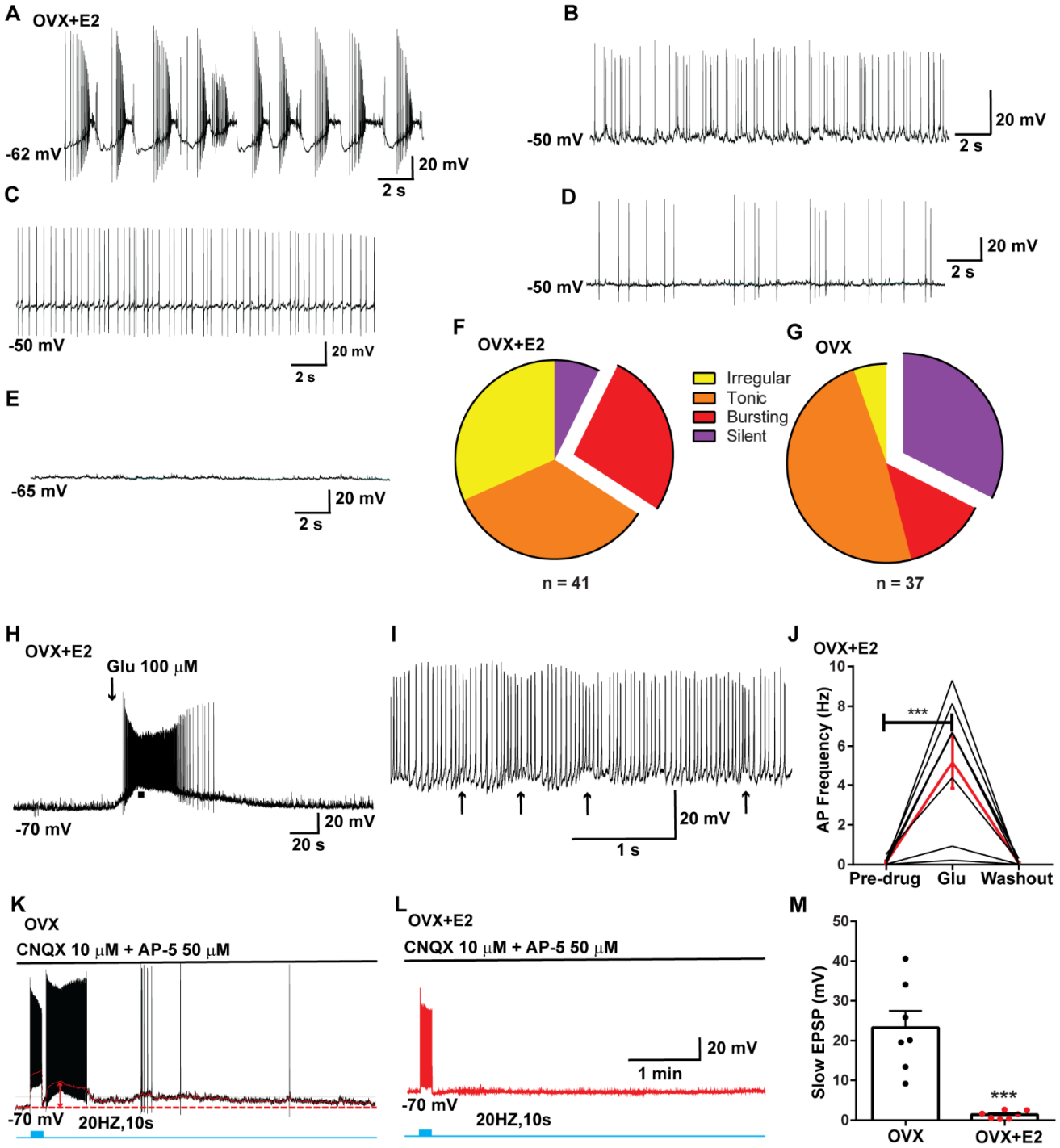

Figure 1. Properties of the firing of Kiss1^{ARH} neurons from OVX and E2-treated OVX mice. **A**–**E**. Representative whole cell, current clamp recordings of spontaneous phasic burst firing (A, which is only seen in E2-treated mice with clear up and down states), irregular burst firing (B), tonic firing (C), irregular firing (D) and silent (E) in Kiss1^{ARH} neurons from E2-treated OVX mice. **F**-**G**. Summary pie chart illustrating the distribution of firing patterns in Kiss1^{ARH} neurons from OVX+E2 (F, from 6 mice) or OVX (G, from 8 mice) mice (OVX versus OVX+E2, Chi-square test, X^2 = 16.05, df = 3, **p = 0.0011). **H**. Current clamp recording in a Kiss1^{ARH} neuron from an OVX+E2 female demonstrating the response to glutamate (100 µM). RMP = -70 mV. Similar responses were observed in all recorded female Kiss1^{ARH} neurons (n = 7 from 4 mice). **I**. The spiking activity above the bar in G was expanded to highlight the pronounced effects of glutamate on burst firing activity of Kiss1^{ARH} neurons, characterized by an ensemble of spikes riding on top of low-threshold spikes (arrows). Drugs were rapidly perfused into the bath as a 4-µl bolus. **J**. Spontaneous AP frequency of Kiss1^{ARH}

neurons before, during, and after glutamate application (n = 7 cells). Data are presented as mean ± SEM. Statistical comparisons between different treatments were performed using one-way ANOVA ($F_{(2, 18)}$ = 14.60, p = 0.0002) followed by Bonferroni's *post hoc* test. *** indicates p < 0.005. **K**-**L**. Representative traces showing the amplitude of slow EPSPs induced by high frequency photostimulation in $Kiss1^{ARH}$ neurons in the presence of ionotropic glutamate receptor antagonists CNQX and AP5 from OVX (K) and OVX+E2 (L) females. The arrows indicate the measurements of slow EPSP amplitude after low-pass filtering (shown in K). **M**. Bar graphs summarizing the slow EPSPs in the $Kiss1^{ARH}$ neurons from OVX and E2-treated OVX mice in the presence of CNQX and AP5. Statistical comparisons between the two groups were performed using an unpaired t-test ($t_{(12)}$ = 5.181, p =0.0002). Data are expressed as mean ± SEM , with data points representing the number of cells.

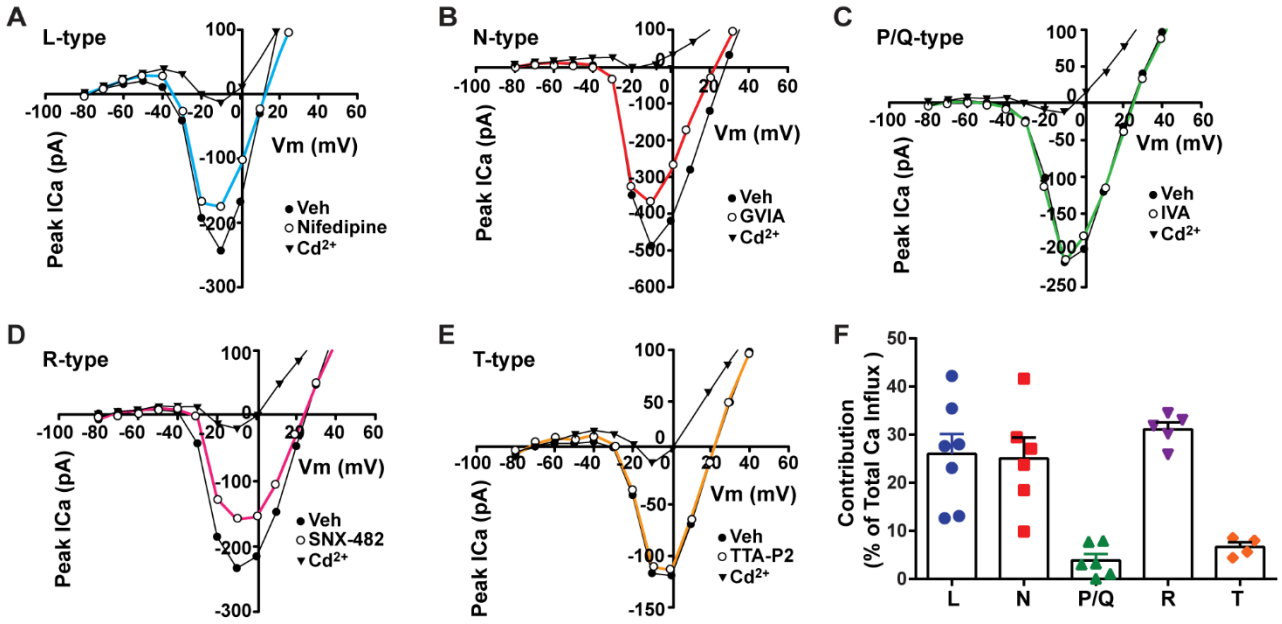

Figure 2. Relative contribution of voltage-gated calcium currents in *Kiss1*^{ARH} neurons from OVX mice. **A-E**, representative current –voltage relationships showing that Cd^{2+} (non-selective blocker of calcium channels) sensitive peak currents were inhibited by different calcium channel blockers: A, nifedipine; B, ω-conotoxin GIVA; C, ω-agatoxin IVA; D, SNX-482; E, TTA-P2. **F**, the maximum peak currents were measured at -10 mV. The proportions of Ca^{2+} currents inhibited by nifidipine (L type), ω-conotoxin GVIA (N type), ω-agatoxin IVA (P/Q), SNX-482 (R type) and TTA-P2 (T type). Data are expressed as mean ± SEM , with data points representing the number of cells.

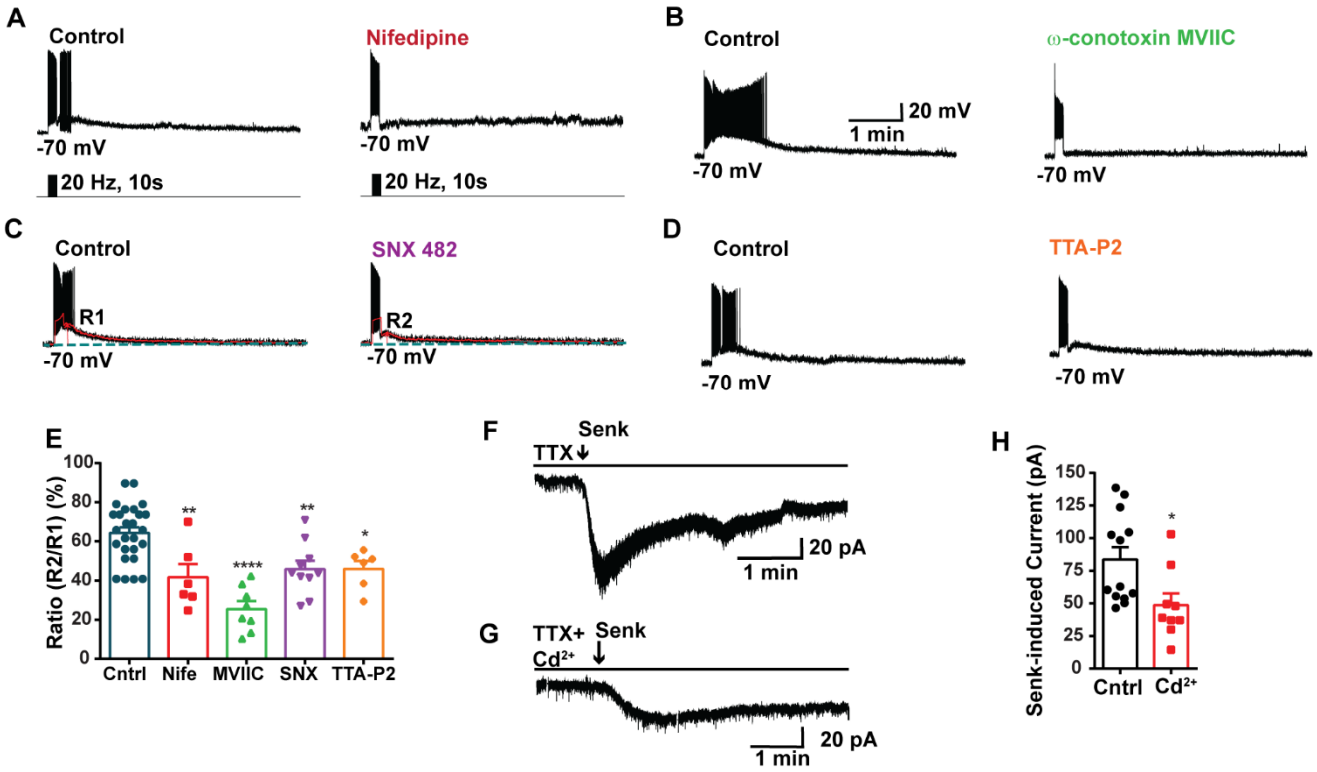

Figure 3. Blockade of HVA Ca^{2+} channels decreases the slow EPSP in *Kiss1^{ARH}* neurons. **A-D**, representative traces showing that the slow EPSPs induced by high frequency photostimulation were abolished by perfusing the blocker of the L-type calcium channel, nifedipine (A) or N- and P/Q -type calcium channels, ω-conotoxin MVIIC (B), or the R-type calcium channel, SNX 482 (C), or the T-type calcium channel, TTA-P2 (D), respectively. The arrows indicate the measurements of slow EPSP amplitude, denoted as R1 and R2, after low-pass filtering (shown in C). **E.** Bar graphs summarizing the effects of drugs on the R2/R1 ratios. The slow EPSP was generated in OVX Kiss1-Cre::Ai32 mice. Comparisons between different treatments were performed using a one-way ANOVA analysis ($F_{(3, 51)} = 14.36$, $p<0.0001$) with the Bonferroni's *post hoc* test. *, **, **** indicates $p < 0.05$, 0.01, 0.001, respectively vs. control. **F**-**G**. Representative traces show that in voltage clamp, senktide induced a significant inward current in Kiss1^{ARH} neurons (F) in the presence of TTX. This current was inhibited by the calcium channel blocker $CdCl_2$ (200 μM)(G) in another cell. **H**. Bar graphs summarize the effect of the calcium channel blocker $CdCl_2$ on the senktide-induced inward currents. Un-paired t-test for F versus G: $t_{(20)} = 2.575$, $p = 0.0181$; * $p < 0.05$. Data are expressed as mean ± SEM, with data points representing the number of cells.

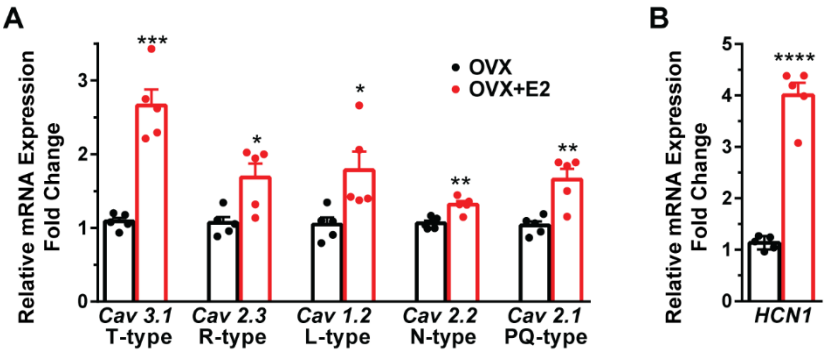

Figure 4 A, E2 increases the expression of low and high voltage-activated calcium channels in Kiss1^{ARH} neurons. Kiss1^{ARH} neurons (three 10-cell pools) were harvested from each of 5 vehicle- and 5 E2-treated, OVX females to quantify ion channel mRNA expression of low and high voltage activated calcium channels as described in the Methods. The analysis included: T-type (Cav3.1) low voltage-activated, as well as the following high-voltage activated channels: R-type (Cav 2.3), L-type (Cav 1.2), N-type (Cav 2.2) and P/Q-type (Cav 2.1) calcium channels. Interestingly, all of these channels were upregulated with E2 treatment, which significantly increased the whole-cell calcium current (see Figure 5). Bar graphs represent the mean ± SEM with data points representing individual animals (oil versus E2, Unpaired t test for *Cav 3.1*, $t_{(8)}$= 7.105, ***p=0.0001; for *Cav 2.3*, $t_{(8)}$ = 3.007, *p = 0.0169; for *Cav 1.2*, $t_{(8)}$= 2.721, *p =0.0262; for *Cav 2.2,* $t_{(8)}$ = 4.001, **p 0.0039; for *Cav 2.1,* $t_{(8)}$ = 4.225, **p =0.0028).**B,** The same Kiss1^{ARH} neuronal pools were also analyzed for mRNA expression of *HCN1* ion channels, and E2 also increased the expression of hyperpolarization-activated, cyclic-nucleotide gated HCN1 channels in Kiss1^{ARH} neurons**.** HCN1 channel mRNA expression was the most highly upregulated by E2 treatment in Kiss1^{ARH} neurons. The expression values were calculated via the ΔΔCT method, normalized to GAPDH and relative to the oil control values. (oil versus E2, Unpaired t test, $t_{(8)}$= 11.450, ****p < 0.0001).

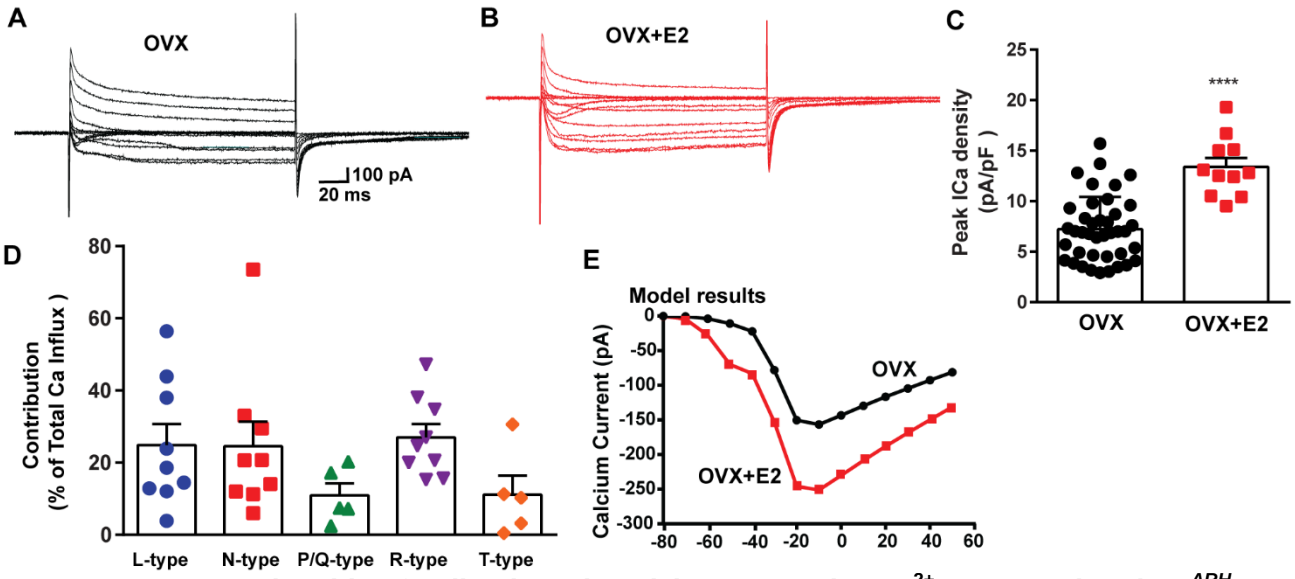

Figure 5. E2 treatment (positive-feedback regimen) increases the Ca^{2+} currents in *Kiss1*^{ARH} neurons. **A-B**, Ca^{2+} currents in *Kiss1*^{ARH} neurons with the same membrane capacitance from oil-treated (A) or E2-treated (B) animals. **C**, the maximum peak currents were measured at -10 mV. The current amplitudes were normalized to the cell capacitance in all cases to calculate current density. The bar graphs summarized the density of Ca^{2+} current in *Kiss1*^{ARH} neurons from oil-treated and E2-treated animals. The mean density was significantly greater in E2-treated (13.4 ± 0.9 pA/pF, n = 11) than in oil-treated OVX females (7.2 ± 0.5 pA/pF, n = 40) (unpaired t-test, $t_{(49)} = 5.75$, ****p < 0.0001). **D.** Relative contribution of voltage-gated calcium currents in *Kiss1*^{ARH} neurons from OVX, E2-treated mice. The maximum peak currents were measured at -10 mV. The proportions of Ca^{2+} currents inhibited by nifidipine (L type), ω-Conotoxin GVIA (N type), ω-agatoxin IVA (P/Q), SNX-482 (R type) and TTA-P2 (T type). Data are expressed as mean ± SEM, with data points representing the number of cells. **E**. The modeling predicts that E2-treated, OVX females exhibit a significantly greater inward Ca^{2+} current (red trace) than the vehicle-treated females (black trace). The coductance of the modelled voltage-gated calcium current (L-, N-, P/Q-, and R-type) is set to 2.1 nS in the OVX state and 2.8 nS in OVX+E2 state, while for the T-type is set to 0.66 nS in the OVX state and 5 nS in OVX+E2 state.

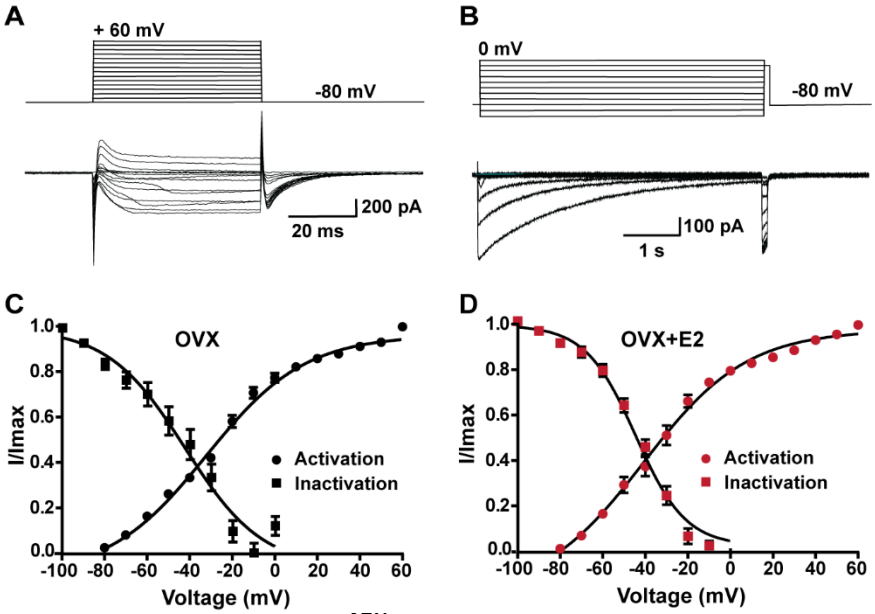

Figure 6. Voltage dependence of I_{Ca} in *Kiss1*^{ARH} neurons from OVX and OVX+E2 mice. A-B, top panels: activation and inactivation protocol. Bottom: representative traces. **C-D**, the mean $V_{1/2}$ values for calcium channel activation were not significantly different for cells from controls versus cells from E2-treated females. Similarly, the $V_{1/2}$ values for channel steady-state inactivation were similar for both groups. Data are expressed as mean ± SEM.

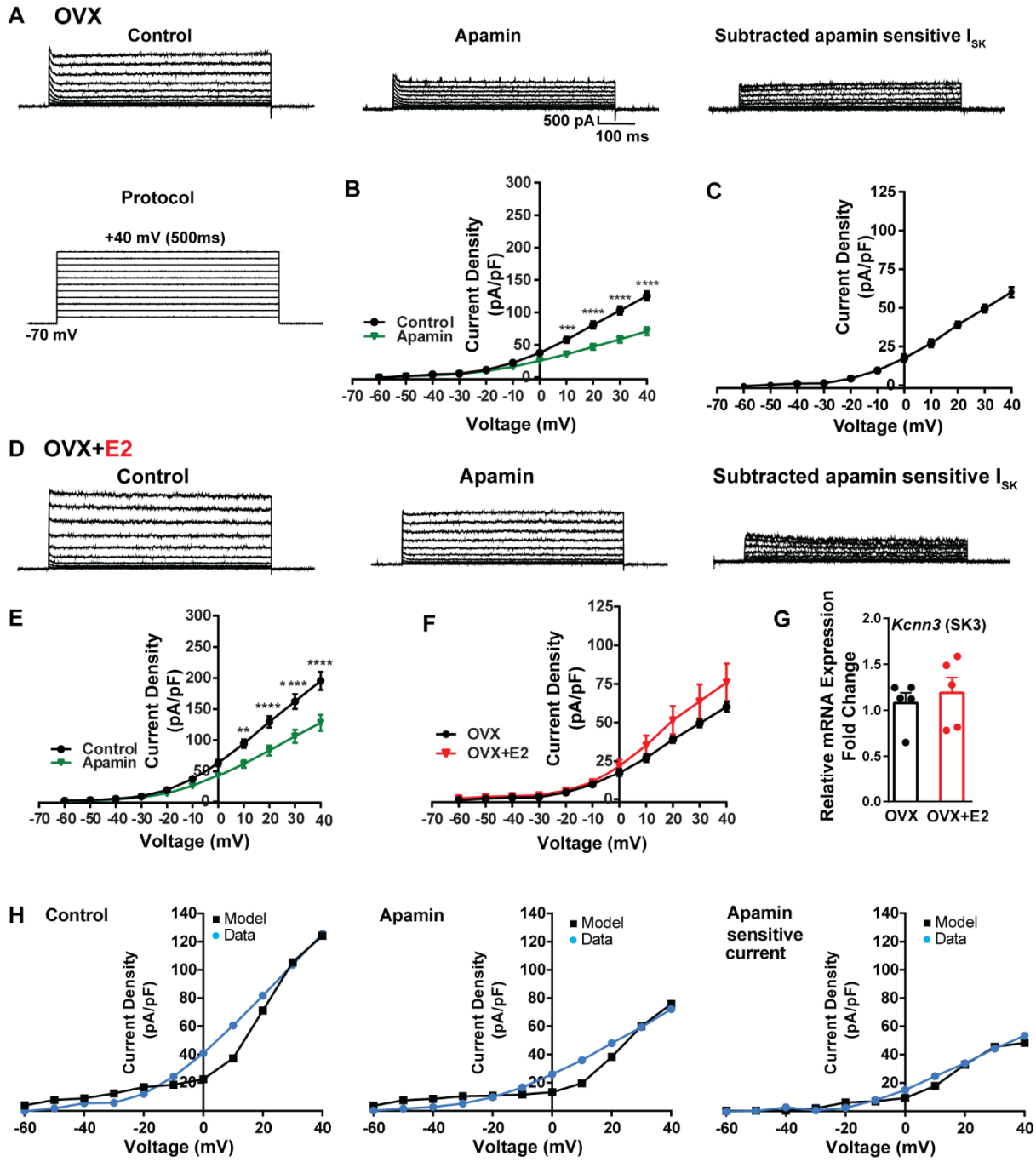

Figure 7. Contribution of Small conductance, calcium-activated K^+ (SK) channel to *Kiss1*^{ARH} neuronal excitability. A. Representative traces of the inhibition of outward currents before (left, control) and after the specific SK blocker Apamin (500 nM, middle). Apamin sensitive currents were calculated from the subtraction of control and apamin at depolarized potentials (right). Cells were clamped at -70 mV and given 500 ms voltage pulses from -60 mV to +40 mV in 10 mV steps at 0.2 Hz, as shown in A at the bottom. **B**. Mean current density-voltage relationships measured at the end of the 500 ms voltage step ranging from -60 mV to +40 mV were obtained in the absence and presence of apamin (two-way ANOVA: main effect of treatment ($F_{(1, 8)} = 22.69$, $p = 0.0014$), main effect of time ($F_{(10, 80)} = 306.0$, $p < 0.0001$) and interaction ($F_{(10, 80)} = 24.76$, $p < 0.0001$); mean ± SEM; n = 5; *post hoc* Bonferroni test, ***p < 0.005, ****p < 0.001). **C**. Apamin sensitive current densities were obtained from B (mean ± SEM, n = 5). **D.** Representative traces of the inhibition of outward currents before (left, control) and after the specific SK blocker Apamin (500 nM, middle). Apamin sensitive currents were resulted from the subtraction of control and apamin at depolarized potentials (right). **E**. Mean current density-voltage relationships measured at the end of the 500 ms voltage step ranging from -60 mV to

+40 mV were obtained in the absence and presence of apamin (two-way ANOVA: main effect of treatment ($F_{(1, 10)}$ = 12.85, p = 0.0050), main effect of time ($F_{(10,100)}$ = 264.1, p < 0.0001) and interaction ($F_{(10, 100)}$ = 11.93, p < 0.0001); mean ± SEM, n = 6; *post hoc* Bonferroni test, **p < 0.01, ****p < 0.001). **F**. Apamin sensitive current densities were obtained from C and E (ns; Two-way ANOVA followed by Bonferroni *post hoc* test; mean ± SEM; OVX, n = 5; OVX+E2, n = 6). **G**. $Kiss1^{ARH}$ neurons (three 10-cell pools) were harvested from each of 5 vehicle- and 5 E2-treated, OVX females to quantify the mRNA expression of SK3 ion channel. E2 did not increase the mRNA expression of small conductance calcium-activated K^+ (SK3) channels in $Kiss1^{ARH}$. Bar graphs represent the mean ± SEM, with data points representing the number of animals, oil versus E2, Unpaired t test, $t_{(8)}$= 0.551, p = 0.5967. The expression values were calculated via the ΔΔCT method, normalized to GAPDH and relative to the oil control values. **H**. The mathematical model was calibrated on the electrophysiology data from $Kiss1^{ARH}$ neurons before and after treatment with the specific SK blocker apamin, left panel versus middle panel respectively. For the calibration it was assumed that the applied concentration of apamin (500nM) completely blocked the SK current. The modeled apamin-sensitive current with g_{SK}=28.1 nS (right panel) matches the electrophysiological data from OVX animals.

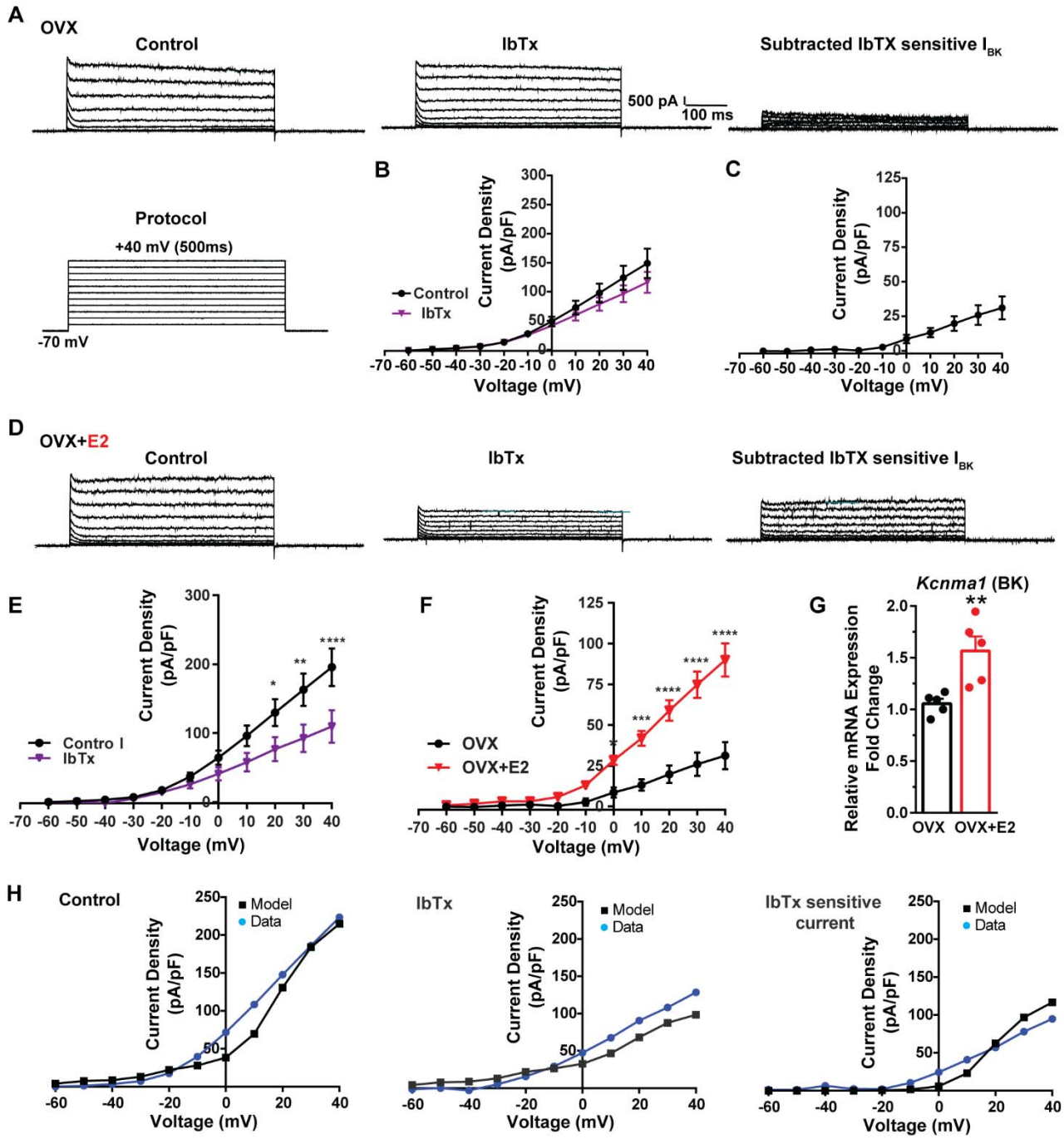

Figure 8. E2 up-regulates *Kcnma1* mRNA and BK current in Kiss1^{ARH} neurons. **A**. Representative traces of the inhibition of outward currents before (left, control) and after the specific BK blocker iberiotoxin (IbTx; 200 nM, middle). IbTx sensitive currents were calculated from the subtraction of control and IbTx at depolarized potentials (right). Cells were clamped at -70 mV and given 500 ms voltage pulses from -60 mV to +40 mV in 10 mV steps at 0.2 Hz, as shown in A at the bottom. **B**. Mean current density-voltage relationships measured at the end of the 500 ms voltage step ranging from -60 mV to +40 mV were obtained in the absence and presence of IbTx (two-way ANOVA: main effect of treatment ($F_{(1, 8)}$ = 0.8841, p = 0.3746), main effect of time ($F_{(10, 80)}$ = 71.56), p < 0.0001) and interaction ($F_{(10, 80)}$ = 1.127, p = 0.3528); mean ± SEM, n = 5; *post hoc* Bonferroni test, p > 0.05). **C**. IbTX sensitive current densities were obtained from B (mean ± SEM, n = 5). **D**. Representative traces of the inhibition of outward currents before (left, control) and after the specific BK blocker iberiotoxin (IbTx; 200 nM, middle). IbTx sensitive currents were resulted from the subtraction of control and IbTx at depolarized potentials (right). **E**. Mean current density-voltage relationships measured at the end of

the 500 ms voltage step ranging from -60 mV to +40 mV were obtained in the absence and presence of IbTX (two-way ANOVA: main effect of treatment ($F_{(1, 10)}$ = 4.660, p = 0.0562), main effect of time ($F_{(10, 100)}$ = 63.98, p < 0.0001) and interaction ($F_{(10, 100)}$ = 4.907, p < 0.0001); mean ± SEM, n = 6; *post hoc* Bonferroni test, *p < 0.05, **p < 0.01, **** < 0.001). **F**. IbTx sensitive current densities were obtained from C and E (two-way ANOVA: main effect of treatment ($F_{(1, 9)}$ = 22.04, p = 0.0011), main effect of time ($F_{(10, 90)}$ = 78.26, p < 0.0001) and interaction ($F_{(10, 90)}$ = 17.84, p <0.0001); mean ± SEM, OVX, n = 5; OVX+E2, n = 6; Bonferroni *post hoc* test, *p < 0.05, ***p < 0.005, ****p < 0.001). **G**. $Kiss1^{ARH}$ neurons (three 10-cell pools) were harvested from each of 5 vehicle- and 5 E2-treated, OVX females to quantify the mRNA expression of BKα channel. E2-treatment increased the mRNA expression of BKα. The expression values were calculated via the ΔΔCT method, normalized to GAPDH and relative to the oil control values. Bar graphs represent the mean ± SEM, with data points representing the number of animals (unpaired two-tailed t-test for BK, $t_{(8)}$ = 3.479, **p = 0.0083). **H**. The mathematical model was calibrated to reproduce the current voltage relationship observed in $Kiss1^{ARH}$ neurons before and after treatment with IbTx. For the calibration it was assumed that the applied concentration of IbTx (200 nM) completely blocked the BK current. The modeled IbTx -sensitive current with g_{BK}=20.0 nS (right panel) matches the electrophysiological data from OVX+E2 animals.

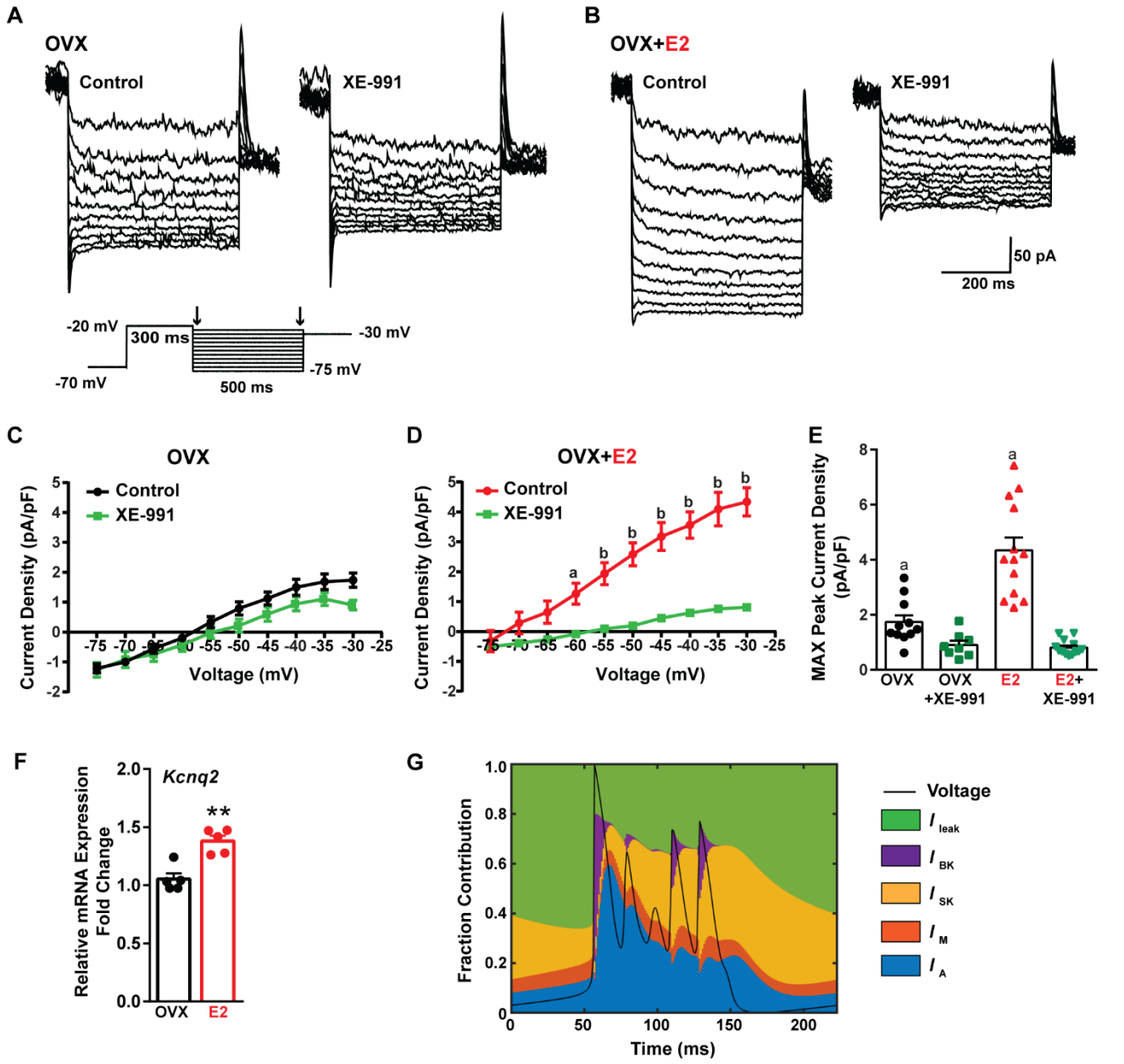

Figure 9. E2 up-regulates KCNQ channels and M-current in *Kiss1*^{ARH} neurons. **A-B**. Representative current traces of the M-current inhibition caused by 40 µM XE-991 perfused for 10 min in (A) OVX-oil and (B) OVX+E2-treated female mice. Inset: M-current deactivation protocol. **C-D**. Current density-voltage plots from –75 to –30 mV of vehicle and XE-991 perfusion in (C) OVX-oil and (D) OVX+E2-treated mice. Two-way ANOVA for C: main effect of treatment ($F_{(1, 17)}$ = 1.908, p = 0.1851), main effect of time ($F_{(9, 153)}$ = 187.1, p < 0.0001), and interaction ($F_{(9, 153)}$ = 3.901, p = 0.0002); Veh, n = 11; XE-991, n = 8; Bonferroni *post hoc* test, p > 0.05. For D: main effect of Veh and XE-991 ($F_{(1, 24)}$ = 24.92, p < 0.0001), main effect of time ($F_{(9, 216)}$ = 174.5, p < 0.0001), and interaction ($F_{(9, 216)}$ = 52.75, p < 0.0001); Veh, n = 13; XE-991, n = 13; Bonferroni *post hoc* test, a = p < 0.05, b = p < 0.001. **E**. Treatment with E2 elevated, while XE-991 diminished the maximum peak current density elicited by a -30 mV step in OVX- and OVX+E2-treated mice. Two-way ANOVA: main effect of Veh and XE-991 ($F_{(1, 41)}$ = 47.59, p < 0.0001), main effect of OVX and OVX+E2 ($F_{(1, 41)}$ = 15.76, p = 0.0003), and interaction ($F_{(1, 41)}$ = 18.2, p = 0.0001; Veh, n = 11; XE-991, n = 8; Bonferroni *post hoc* test, Veh: OVX vs. OVX+E2, a = p < 0.001. XE-991: OVX vs. OVX+E2, p > 0.05. Data are expressed as mean ± SEM, with data points representing the number of cells. **F**. Kiss1^{ARH} neurons (three10-cell pools) were harvested from each of 5 vehicle- and 5 E2-treated, OVX females to quantify the mRNA expression of *Kcnq2*. E2 treatment increased the mRNA expression of *Kcnq2*. Unpaired t-test, $t_{(8)}$ = 4.850, **p = 0.0013. Data are expressed as mean ±

SEM, with data points representing the number of animals. **G**. Percent contribution of the different K^+ currents to the repolarization current during burst-type firing activity in the OVX+E2 state. At each time point, the length of each color bar denotes the percent contribution of the corresponding current to the total outward current.

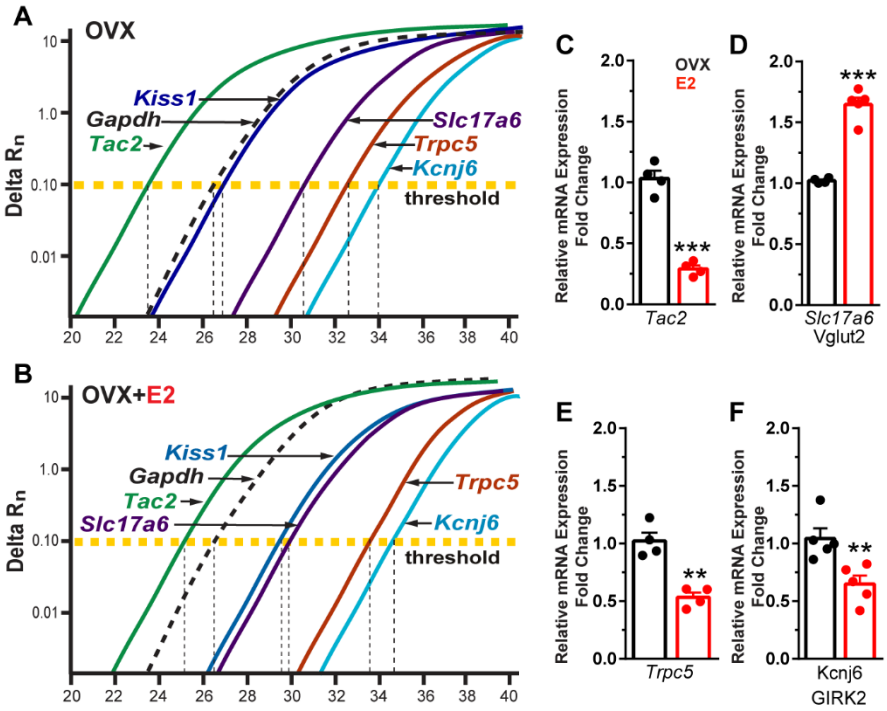

Figure 10. Estradiol decreases *Tac 2, Trpc5 and Kcnj6* but increases *Vglut 2* mRNA expression in Kiss1^{ARH} neurons. **A.** qPCR amplification curves illustrating the cycle threshold (CT) for *Tac2, Gapdh, Kiss1*, *Trpc5, Slc17a6 (Vglut2) and Kcnj6* (*GIRK2)* in Kiss1^{ARH} ten cell neuronal pools (three to six pools from each animal) in OVX Oil-treated, and **B,** in OVX E2-treated females. **C.** Quantitative real-time PCR analysis of *Tac2* mRNA, **D**, *Vglut2*, **E,** *Trpc5*, **F,** *Kcnj6*. Comparisons were made between Oil-treated and E2-treated, OVX females using the comparative $2^{-\Delta\Delta CT}$ method. Bar graphs represent the mean ± SEM, with data points representing the number of animals. (Unpaired t test for *Tac2*, $t_{(6)} = 10.670$, ***p < 0.0001; for *Vglut2*, $t_{(7)} = 9.678$, ***p < 0.0001; for *Trpc5*, $t_{(6)} = 5.774$, **p = 0.0012; for *Kcnj6,* $t_{(8)} = 3.457$, **p = 0.0086).

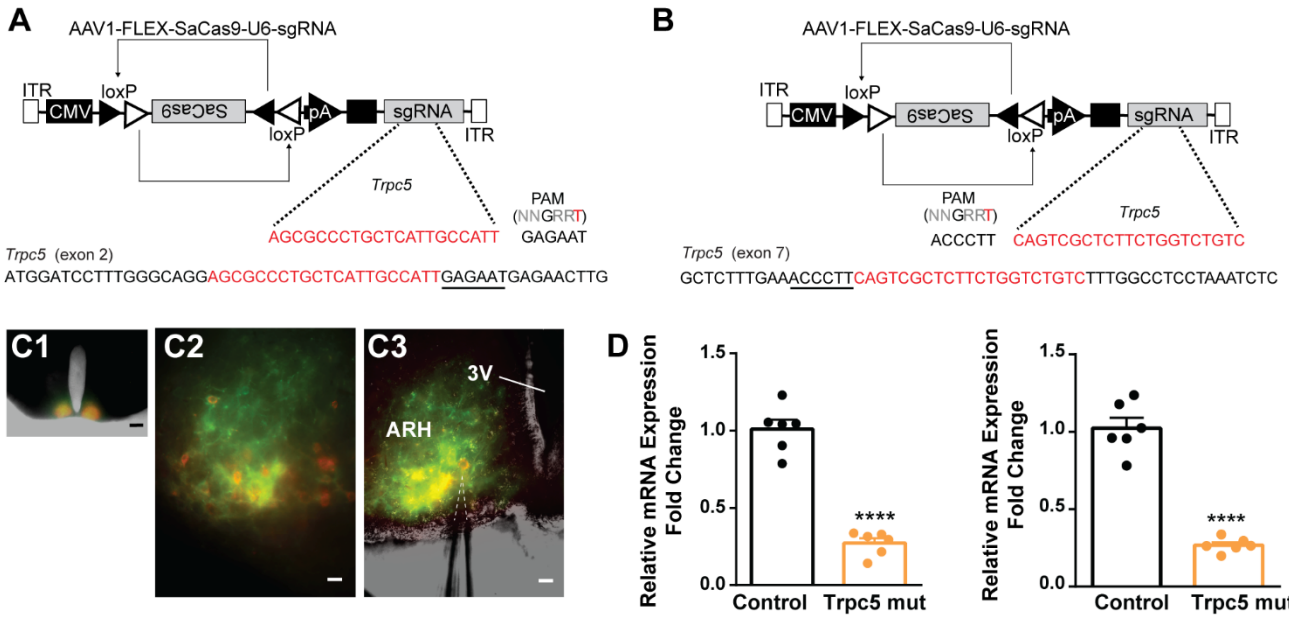

Figure 11. CRISPR mutagenesis of *Trpc5* channels in Kiss1^{ARH} neurons. **A**, structure of AAV1-FLEX-SaCas9-U6sg*Trpc5-exon2*. Exon 2 of *Trpc5* is denoted with guide sequence highlighted in red, the PAM is underlined. **B**. Structure of AAV1-FLEX-SaCas9-U6sg*Trpc5-exon7*. Exon 7 of *Trpc5* is denoted with guide sequence highlighted in red, the PAM is underlined. **C1**, image of coronal section through the ARH from Kiss1-Cre::Ai32 mouse with dual co-injections of AAV-DIO-mCherry and AAV1-FLEX-SaCas9-U6-sg*Trpc5*. Scale = 200 µm. **C2, C3**, higher power overlays of epifluorescence (EYFP & mCherry) images with recording pipette patched onto a Kiss1^{ARH}-Cre:mCherry cell (C3). Scale = 40 µm. **D**, quantitative PCR measurements of *Trpc5* transcripts from 10 cell neuronal pools (three pools from each animal) in double sgRNA mutagenesis of *Trpc5* (second sgRNA against pore forming region) in Kiss1^{ARH} neurons. Primers were targeted to 1st (left panel) or 2nd (right panel) guide, respectively (Unpaired t test for 1st, $t_{(10)} = 10.67$, ****$p < 0.0001$; for 2nd, $t_{(10)} = 10.79$, ****$p < 0.0001$). Data are expressed as mean ± SEM, with data points representing the number of animals.

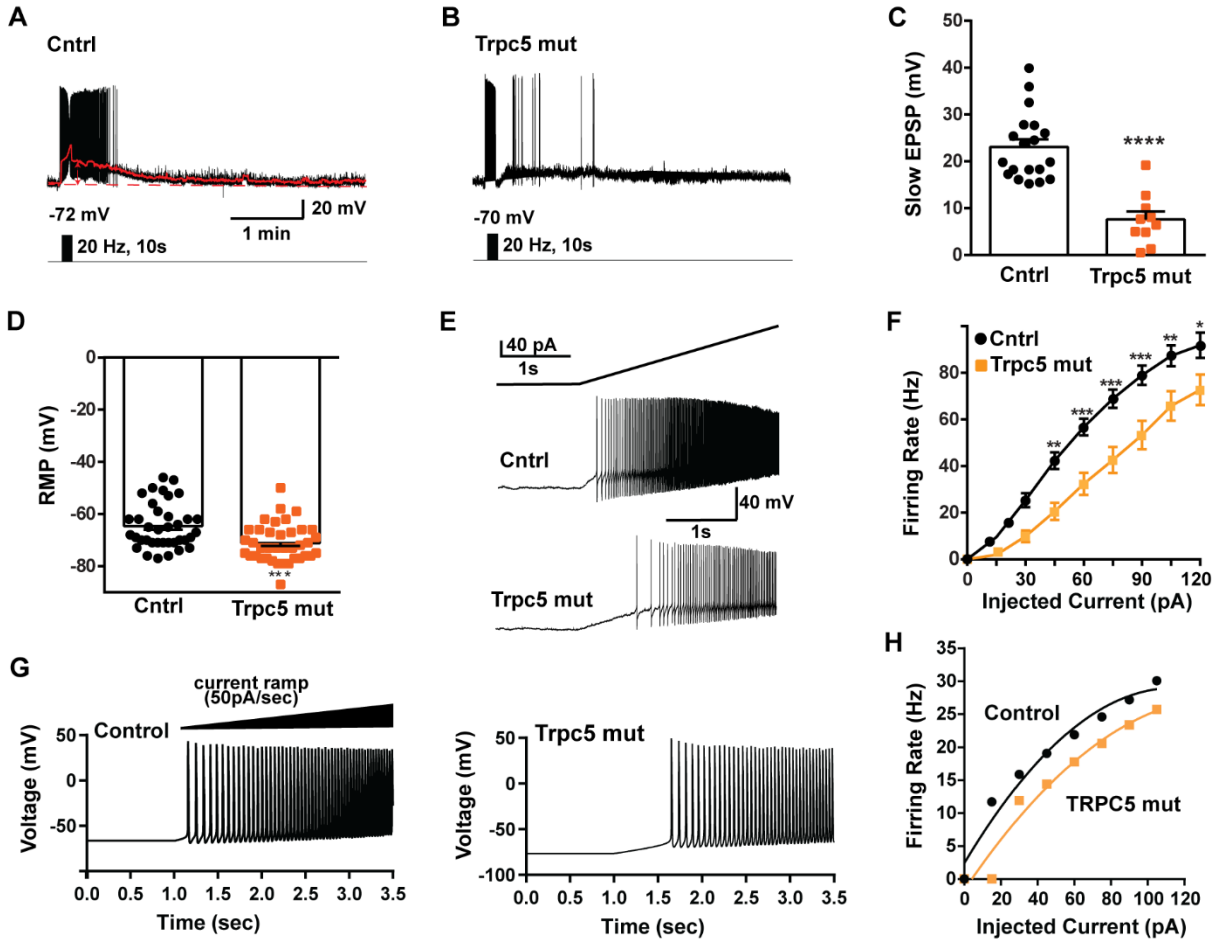

Figure 12. Double CRISPR mutagenesis of *Trpc5 attenuates slow EPSP,* increases rheobase and shifts the F-I curve. A, high-frequency photo-stimulation (20 Hz) generated slow EPSP in Kiss1^{ARH} neuron from ovariectomized, control mouse. Red trace is slow EPSP after low-pass filtering**. B**, slow EPSP in Kiss1^{ARH} neuron from OVX, double sg*Trpc5* -targeted (*Trpc5* mut) mouse. **C**, summary of the effects of *Trpc5* mutagenesis on slow EPSP amplitude in female mice. Unpaired t-test, $t_{(27)} = 5.916$, ****p < 0.0001. Data are expressed as mean ± SEM, with data points representing the number of cells. **D**, double sgRNA mutagenesis of *Trpc5* channels in Kiss1^{ARH} neurons significantly increased the RMP (control: -64.5 ± 1.4 mV versus *Trpc5* mut, 2: -71.1 ± 1.2 mV, Unpaired t-test, $t_{(73)} = 3.524$, ***p = 0.0007). **E**, current ramp showing the increased rheobase in Kiss1^{ARH} neuron from Trpc5 mut mice (control: 31.1 ± 1.2 pA, n = 31, versus *Trpc5* mut , 35.3 ± 1.0 pA, n = 33, Unpaired t-test, $t_{(62)} = 2.777$, **p = 0.0073). **F**, firing frequency vs. current (F-I) curves for control versus *Trpc5* mut (two-way ANOVA: main effect of treatment, $F_{(1,52)} = 13.03$, p = 0.0007, main effect of time, $F_{(8,416)} = 291.3$, p < 0.0001, and interaction, $F_{(8,416)} = 6.254$, p < 0.0001; Control, n = 26, *Trpc5* mut, n = 29; *post hoc* Bonferroni test, *<0.05; **<0.01 and ***p < 0.005, respectively). **G**, model simulations of the effects of a current ramp (50 pA/sec) for OVX (left panel) and OVX female with reduced (muted) TRPC5 conductance (right panel), and **H**, the associated firing frequency vs. current curves. In the latter case the TRCP5 conductance was halved, which is a conservative estimation of the CRISPR state in which the *Trpc5* is much more mutated in Kiss1^{ARH} neurons (Figure 11).

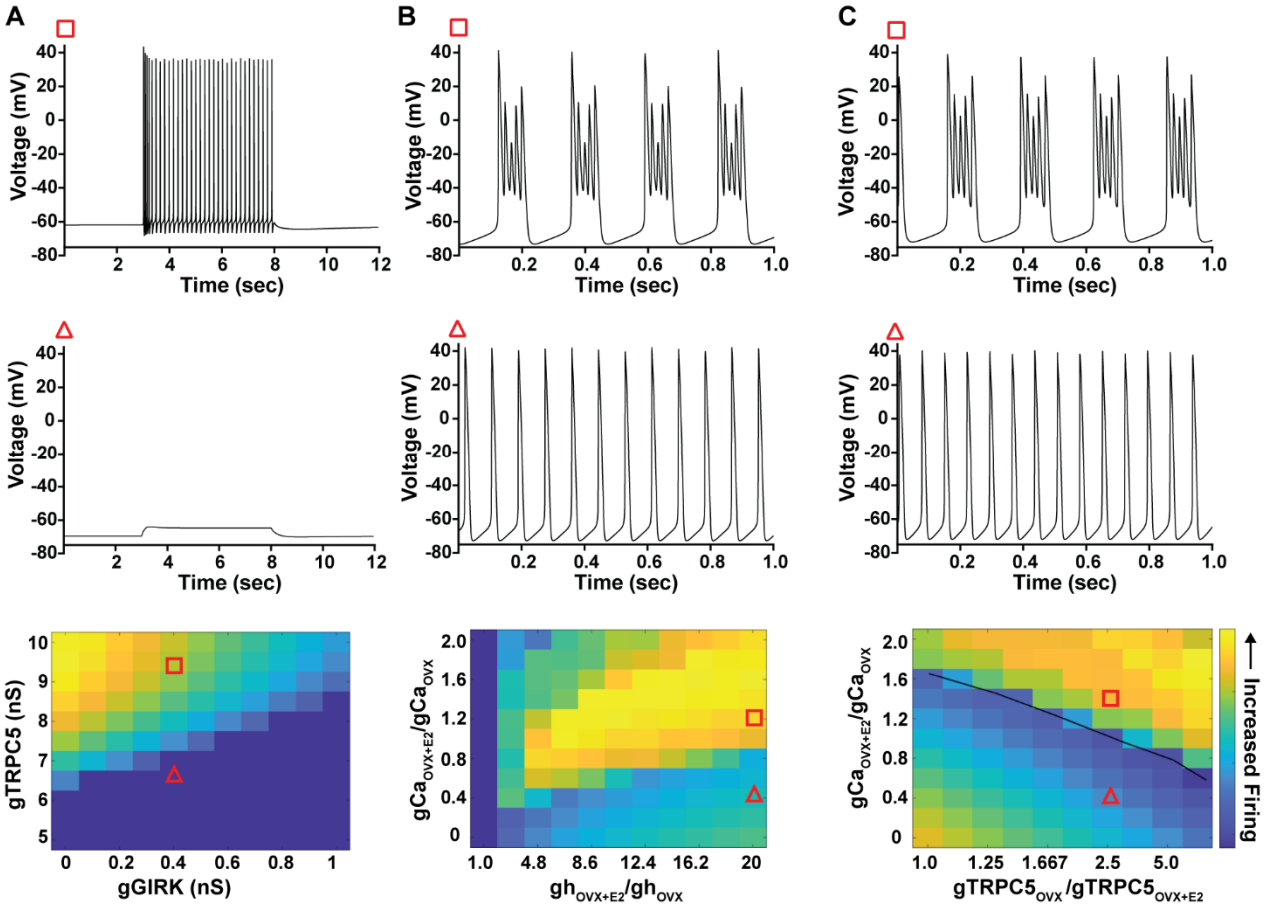

Figure 13. Computational modeling of a Kiss1^{ARH} neuron in the OVX and OVX + E2 state demonstrates its distinct dynamic responses. A model of the Kiss1^{ARH} neuron was developed and calibrated using molecular data and electrophysiological recordings of Kiss1^{ARH} neurons from OVX and OVX+E2 mice. **A.** Simulations of the OVX-parameterized model demonstrating high frequency activity in response to saturating levels of NKB stimulation. The balance between GIRK and TRCP5 conductance controls the response of the neuron to NKB stimulation, with neuronal response eliminated when TRPC5 conductance is low (red triangle) relative to the GIRK conductance. **B.** The OVX+E2 parameterized models demonstrate sustained burst firing activity. The bursting activity that is supported by elevated h- and Ca $^{2+}$-currents (red square) as observed in OVX+E2 mice. **C.** In the OVX+E2 state, burst firing activity is also supported by high conductance of HVA Ca^{2+} channels relative to the conductance of TRPC5 channels. Representative points in the parameter space giving rise to burst firing activity are marked with red squares, whereas red triangles are used for points resulting in regular spiking. The black line separates these two regions of activity.

Supplemental Information:

A mathematical model of the arcuate nucleus kisspeptin neuron

A schematic diagram of the Arcuate nucleus Kiss1 (Kiss1^{ARH}) neuron model is presented in Fig. S1 and parameter values used in the simulations are given in Table S1.

The equation describing the membrane potential, V_m, of Kiss1^{ARH} neurons is given by

$$C_m \frac{dV_m}{dt} = -I,$$

where C_m is the membrane capacitance and I is the sum of 12 ionic currents:

$$I = I_{NaT} + I_{NaP} + I_A + I_{BK} + I_h + I_{SK} + I_M + I_T + I_{Ca} + I_{TRPC5} + I_{GIRK} + I_{leak}$$

I_{NaT} and I_{NaP} are the transient and persistent sodium currents, respectively; I_A represents the A current; I_M represents the M current; I_{SK} and I_{BK} are the potassium currents through the SK and BK channels respectively; I_T the T-type calcium current; I_{Ca} represents other calcium currents (L-, N-, P/Q-, and R-type); I_{TRPC5} represents Calcium current through the TRPC5 channel; I_{GIRK} potassium current through the GIRK channels. Finally, I_{leak} represents the contribution of leak currents.

We use the Hodgkin-Huxley formalism to model current dynamics and their dependence on the membrane potential. Below we detail are the equations governing the currents.

Transient sodium current

$$I_{NaT} = g_{NaT} \cdot m_{NaT,\infty}(V_m) \cdot h_{NaT} \cdot (V_m - E_{Na}),$$

where g_{NaT} is the maximum conductance; E_{Na} is the sodium reversal potential; h_{NaT} is the inactivation gating variable that obeys the following equation:

$$\frac{d\,h_{NaT}}{dt} = \frac{h_{NaT,\infty}(V_m) - h_{NaT}}{\tau_{h,NaT}}.$$

Parameter $\tau_{h,NaT}$ dictates the timescale of inactivation and $h_{NaT,\infty}(V_m)$ is the steady-state inactivation function:

$$h_{NaT,\infty}(V_m) = \frac{1}{1+e^{-(V_m - V_{h,NaT})/k_{h,NaT}}}.$$

Parameter $V_{h,NaT}$ describes the voltage achieving half-maximal inactivation and parameter $k_{h,NaT}$ is the associated scaling function.

Finally, in the current formulation $m_{NaT,\infty}(V_m)$ is the steady-state activation function given by:

$$m_{NaT,\infty}(V_m) = \frac{1}{1+e^{-(V_m - V_{m,NaT})/k_{m,NaT}}}.$$

The transient sodium channel is modelled using parameter values from the Purkinje neuron [1]. This neuron was chosen as a baseline as it contains the same subunits, i.e., NaV1.1-α, NaV1.2-α, and NaV1.6-α [1], as the transient sodium channel in Kiss1^{ARH} neuron [2].

Persistent sodium current:

$$I_{NaP} = g_{NaP} \cdot m_{NaP,\infty}(V_m) \cdot h_{NaP} \cdot (V_m - E_{Na}),$$

g_{NaP} is the maximum conductance; h_{NaP} is the corresponding inactivation gating variable that obeys the following equation:

$$\frac{dh_{NaP}}{dt} = \frac{h_{NaP,\infty}(V_m) - h_{NaP}}{\tau_{h,NaP}};$$

and the steady-state activation and inactivation functions are given by:

$$m_{NaP,\infty}(V_m) = \frac{1}{1 + e^{-(V_m - V_{m,NaP})/k_{m,NaP}}},$$

$$h_{NaT,\infty}(V_m) = \frac{1}{1 + e^{-(V_m - V_{h,NaP})/k_{h,NaP}}}.$$

The above description of the persistent sodium current was taken from a model of the GnRH neuron [3].

A current:

$$I_A = g_A \cdot m_A \cdot h_A \cdot (V_m - E_K)$$

g_{NaP} denotes the maximum conductance; E_K is the potassium reversal potential; and m_A and h_A are the corresponding activation and inactivation gating variables, which are described by the following equations:

$$\frac{dm_A}{dt} = \frac{m_{A,\infty}(V_m) - m_A}{\tau_{m,A}};$$

$$\frac{dh_A}{dt} = \frac{h_{A,\infty}(V_m) - h_A}{\tau_{h,A}}.$$

The steady-state activation and inactivation functions are given by:

$$m_{A,\infty}(V_m) = \frac{1}{1 + e^{-(V_m - V_{m,A})/k_{m,A}}},$$

$$h_{A,\infty}(V_m) = \frac{1}{1 + e^{-(V_m - V_{h,A})/k_{h,A}}}.$$

The model of the A-current was based on Mendonca's model of Kv4 channels [4], as these channels are also found in Kiss1^{ARH} neurons [5].

BK current

$$I_{BK} = g_{BK} \cdot b_{BK,\infty}(V_m, c) \cdot (V_m - E_K),$$

Here, g_{BK} is the maximum conductance; and $b_{BK,\infty}(V_m, c)$ is the steady-state activation function that depends on the membrane potential, V_m, as well as on the cytosolic calcium concertation, c:

$$b_{BK,\infty}(V_m, c) = \frac{1}{1 + e^{-(V_m - V_{BK}(c))/k_{BK}}},$$

$$V_{BK}(c) = V_{BK,0} - k_{shift} \log \frac{c}{k_{c,BK}}.$$

The model of the BK-current was based on the model presented in [6], with the conductance parameter fitted to the current-voltage relationships recorded from Kiss1^{ARH} neurons in the absence and presence of the specific BK blocker, iberiotoxin.

SK current

$$I_{SK} = g_{SK} \cdot b_{SK,\infty}(c) \cdot (V_m - E_K)$$

g_{SK} denotes the maximum conductance; and $b_{SK,\infty}(c)$ is the steady-state activation function, which depends on the cytosolic calcium concertation, c:

$$b_{SK,\infty}(c) = \frac{c^n}{c^n + K_{SK}^n}.$$

The model of the BK-current was based on the model presented in [7], with the conductance fitted to the current-voltage relationships recorded from Kiss1^{ARH} neurons in the absence and presence of the specific SK blocker, apamin.

M current

$$I_M = g_M \cdot m_M \cdot (V_m - E_K)$$

g_M denotes the maximum conductance, and m_M is the corresponding activation gating variable:

$$\frac{dm_M}{dt} = \frac{m_{M,\infty}(V_m) - m_M}{\tau_{m,M}}$$

with the steady-state activation function, $m_{M,\infty}(V_m)$, taking the form:

$$m_{A,\infty}(V_m) = \frac{1}{1 + e^{-(V_m - V_{m,A})/k_{m,A}}}.$$

The model of the M-current was parameterised using the steady-state voltage-clamp measurements from actuate Kiss1 neurons [8], while for the activation timescale we used the timescale used in a model of the CA1/3 pyramidal cells [9].

h current

$$I_h = g_h \cdot \left[p_h \cdot m_{h,1} + (1 - p_h) \cdot m_{h,2}\right] \cdot (V_m - E_h),$$

g_h denotes the maximum conductance; and $m_{h,1}$ and $m_{h,2}$ are separate activation gating variables operating on different timescales ($\tau_{m,h,1}$ and $\tau_{m,h,2}$ respectively):

$$\frac{dm_{h,1}}{dt} = \frac{m_{h,1,\infty}(V_m) - m_{h,1}}{\tau_{m,h,1}}$$

$$\frac{dm_{h,2}}{dt} = \frac{m_{h,2,\infty}(V_m) - m_{h,2}}{\tau_{m,h,2}}$$

The corresponding steady-state activation functions are:

$$m_{h,1,\infty}(V_m) = \frac{1}{1 + e^{-(V_m - V_{m,h,1})/k_{m,h,1}}},$$

$$m_{h,2,\infty}(V_m) = \frac{1}{1 + e^{-(V_m - V_{m,h,2})/k_{m,h,2}}}.$$

Finally, parameter p_h dictates the relative contribution of and $m_{h,1}$ and $m_{h,2}$ to the total current.

This model of the h-current is based on the hippocampal CA1 pyramidal neuron [7].

T-type calcium current

$$I_T = g_T \cdot m_{T,\infty} \cdot \left[p_T \cdot h_{T,1} + (1 - p_T) \cdot h_{T,2}\right] \cdot (V_m - E_{Ca}),$$

g_T is the maximum conductance; and $h_{T,1}$ and $h_{T,2}$ are separate inactivation gating variables operating on different timescales ($\tau_{h,T,1}$ and $\tau_{h,T,2}$ respectively):

$$\frac{dh_{h,1}}{dt} = \frac{h_{T,1,\infty}(V_m) - h_{T,1}}{\tau_{h,T,1}}$$

$$\frac{dh_{h,2}}{dt} = \frac{h_{T,2,\infty}(V_m) - h_{T,2}}{\tau_{h,T,2}}$$

The corresponding steady-state inactivation functions are:

$$h_{T,1,\infty}(V_m) = \frac{1}{1 + e^{-(V_m - V_{h,T,1})/k_{h,T,1}}},$$

$$h_{T,2,\infty}(V_m) = \frac{1}{1 + e^{-(V_m - V_{h,T,2})/k_{h,T,2}}}.$$

The steady-state activation function is given by:

$$m_{T,\infty} = \frac{1}{1 + e^{-(V_m - V_{m,T})/k_{m,T}}}.$$

Finally, parameter p_T dictates the relative contribution of and $h_{T,1}$ and $h_{T,2}$ to the total current.

To model of the T-current was based on AVPV kisspeptin neurons data presented in [2, 10].

L-, N-, P/Q-, R-type calcium currents

$$I_{Ca} = g_h \cdot m_{Ca} \cdot h_{Ca} \cdot (V_m - E_{Ca})$$

g_{Ca} denotes the maximum conductance; and m_{Ca} and h_{Ca} are the corresponding activation and inactivation gating variables, which are described by the following equations:

$$\frac{dm_{Ca}}{dt} = \frac{m_{Ca,\infty}(V_m) - m_{Ca}}{\tau_{m,Ca}};$$

$$\frac{dh_{Ca}}{dt} = \frac{h_{Ca,\infty}(V_m) - h_{Ca}}{\tau_{h,Ca}}.$$

The steady-state activation and inactivation functions are given by:

$$m_{Ca,\infty}(V_m) = \frac{1}{1 + e^{-(V_m - V_{m,Ca})/k_{m,Ca}}},$$

$$h_{Ca,\infty}(V_m) = \frac{1}{1 + e^{-(V_m - V_{h,Ca})/k_{h,Ca}}}.$$

Parameters of the model for the high voltage activated calcium channels were calibrated from the current-voltage relationships obtained from Kiss1^{ARH} neurons (see Figure 2 and 6 of the main text).

TRPC5 current

$$I_{TRPC5} = g_{TRPC5} \cdot b_{TRPC5}(c, R_{TRPC5,act}) \cdot (V_m - E_{TRPC5})$$

g_{TRPC5} denotes the maximum conductance; and $b_{TRPC5}(c, R_{TRPC5,act})$ the activating gating variable that depends both on cytosolic calcium concertation (c) and on NKB-mediated activation of an intermediary effector, $R_{TRPC5,act}$ [11]:

$$b_{TRPC5}(c, R) = \frac{R_{TRPC5,act}}{1 + e^{-(c - c_{TRPC5})/k_{TRPC5}}}$$

The dynamics of $R_{TRPC5,act}$ (activated form of R_{TRPC5}) are described by:

$$\frac{dR_{TRPC5,act}}{dt} = \left(k_{R_{TRPC5},0} + k_{R_{TRPC5}} \frac{NKB^{n2}}{NKB^{n2} + K_{NKB}^{n2}}\right) \cdot (R_{TRPC5,T} - R_{TRPC5,act}) - k_{-R_{TRPC5}} \cdot R_{TRPC5,act};$$

where NKB is the extracellular NKB concertation; $k_{R,0}$ is the basal rate of R_{TRPC5} activation; k_R is the maximal rate of R_{TRPC5} activation in the presence of NKB; k_{-R} is the rate of R_{TRPC5} inactivation; and $R_{TRPC5,T}$ is the total concentration of the effector.

GIRK current

$$I_{GIRK} = g_{GIRK} \cdot b_{GIRK}(V_m, R_{GIRK,act}) \cdot (V_m - E_K)$$

g_{GIRK} denotes the maximum conductance; and $b_{GIRK}(V_m, R_{GIRK,act}B)$ the activating gating variable that depends on membrane potential, V_m, and on external activation of an intermediary effector, $R_{GIRK,act}$:

$$b_{GIRK}(V_m, R_{GIRK,act}) = m_{GIRK}(V_m)\, R_{GIRK,act}(s)$$

The dynamics of m_{GIRK} are described by:

$$\frac{dm_{GIRK}}{dt} = \frac{m_{GIRK,\infty}(V_m) - m_{GIRK}}{\tau_{GIRK}(V_m)}$$

where the steady state activation function and timescale function are given by:

$$m_{GIRK,\infty}(V_m) = \frac{1}{1+e^{-\frac{V_m - V_{GIRK}}{k_{GIRK,1}}}} + \frac{\alpha}{1+e^{-\frac{V_m - V_{GIRK}}{k_{GIRK,2}}}}$$

$$\tau_{GIRK}(V_m) = \frac{1}{\alpha_\tau e^{-(V_m/V_{GIRK})} + \beta_\tau e^{-(V_m/V_{GIRK})}}$$

The dynamics of $R_{GIRK,act}$ are described by:

$$\frac{dR_{GIRK,act}}{dt} = \left(k_{R_{GIRK},0} + k_{R_{GIRK}} \frac{s^{n3}}{s^{n3} + K_s^{n3}}\right) \cdot (R_{GIRK,T} - R_{GIRK,act}) - k_{-R_{GIRK}} \cdot R_{GIRK,act} ;$$

where s is the extracellular concertation of the activation signal.

The model and parameters of the GIRK current is taken from [12].

Leak currents

$$I_{leak} = I_{leak,0} + I_{leak,Ca} = g_{leak,1} \cdot (V_m - E_K) + g_{leak,2} \cdot (V_m - E_{Ca})$$

The leak current parameters were calibrated to current-voltage relationships recorded from Kiss1^{ARH} neurons in the absence/presence of iberiotoxin (BK blocker) and apamin (SK blocker).

Intracellular calcium dynamics

Finally, the intracellular calcium dynamics are described via the following equation:

$$\frac{dc}{dt} = -\left(I_{Ca} + I_T + I_{TRPC5} + I_{leak,Ca}\right) \cdot \gamma - d_{ca} \cdot c$$

where parameter γ converts the currents to molecule fluxes and parameter d_{ca} dictates the linear rate at which calcium is depleted or pumped out of the cell.

Modelling the effect of E2

The effect of E2 on ionic currents is modelled as a change in the maximum conductance parameter. For currents I_M, I_T, I_{Ca} and I_{TRPC5} this change is inferred from the qPCR data assuming that the conductance is directly proportional to the mRNA expression. For I_{SK}, I_{BK}, I_{leak}, the OVX and OVX+E2 conductances are obtained from current-voltage relationships recorded from Kiss1^{ARH} neurons in the absence/presence of iberiotoxin (BK blocker) and apamin (SK blocker). All other currents were assumed to be unaffected by E2. Parameter C_m in calibrated using direct measurements of the membrane conductance in the OVX and OVX+E2 state. For the simulation presented in the Figure 13 of the main text, conductances were varied within ranges that captures the physiological effect of E2.

Computer simulations

Integration of the differential equations describing the model was carried out in MATLAB R2023b using a standard 4th order Runge-Kutta method. Parameter fitting was also conducted in MATLAB R2023b using the least squares curve fitting method.

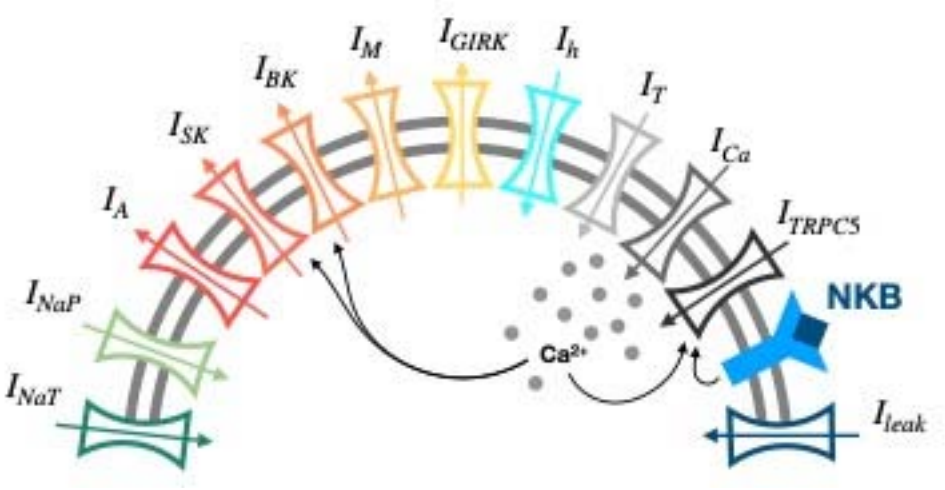

Figure S1. Schematic diagram of the conductance based mathematical model of Arcuate nucleus Kiss1 neurons.

Model parameters					
C_m	23.13 nF (19.5 in OVX+E2)				
Current parameters [1]					References
I_{NaT}	$\tau_{h,NaT}$	4.5 ms	$V_{h,NaT}$	-43.2 mV	[1, 2]
	$V_{m,NaT}$	-25 mV	$k_{m,NaT}$	3 mV	
	$k_{h,NaT}$	-8.2 mV	g_{NaT}	90 nS	
	E_{Na}	66.1 mV			
I_{NaP}	$\tau_{h,NaP}$	250 ms	$V_{h,NaP}$	-47.4 mV	[3]
	$V_{m,NaP}$	-41.5 mV	$k_{m,NaP}$	3 mV	
	$k_{h,NaP}$	-8.5 mV	g_{NaP}	3.37 nS	
	E_{Na}	66.1 mV			

[1] Parameters $g_{\cdot}$ denote the maximum conductance associated with each current.

I_A	$\tau_{h,A}$	10 ms	$V_{h,A}$	-55.1 mV	[4, 5]
	$\tau_{m,A}$	20 ms	$V_{m,A}$	-30 mV	
	$k_{h,A}$	-11.4 mV	$k_{m,A}$	10 mV	
	g_A	60 nS in OVX 35 in OVX+E2	E_K	-81 mV	
I_{BK}	k_{BK}	10 mV	k_{shift}	18 mV	[6]
	$V_{BK,0}$	-22.52 mV	$k_{c,BK}$	1.5 µM	
	g_{BK}	13.50 nS in OVX; 20 nS in OVX+E2	E_K	-81 mV	
I_{SK}	K_{SK}	0.45 µM	n	4	[13]
	g_{SK}	28.13 nS in OVX; 26.05 nS in OVX+E2	E_K	-81 mV	
I_M	$\tau_{m,M}$	10 ms	$V_{m,M}$	-50 mV	[8, 9]
	$k_{m,M}$	20 mV	g_M	0.23 nS in OVX 1.23 ns in OVX+E2	
	E_K	-81 mV			
I_h	$\tau_{m,h,1}$	80 ms	$V_{m,h,1}$	-102 mV	[7, 14, 15]
	$\tau_{m,h,1}$	310 ms	$V_{m,h,2}$	-102 mV	
	p_h	0.85	$k_{m,h,1}$	-10 mV	
	$k_{m,h,2}$	-10 mV	g_h	0.56 nS (11.23 nS in OVX+E2)	
	E_h	-27.8 mV			
I_T	$\tau_{h,T,1}$	1.94 ms	$V_{h,T,1}$	-69.1 mV	[2, 10]
	$\tau_{h,T,2}$	86.3 ms	$V_{h,T,2}$	-69.1 mV	
	p_h	0.5	$V_{m,T}$	-54 mV	
	$k_{h,T,1}$	-5.3 mV	$k_{h,T,2}$	-5.3 mV	

	$k_{m,T}$	3.3 mV	g_T	0.66 nS (5 nS in OVX+E2)	
I_{Ca}	$\tau_{h,Ca}$	10 ms	$V_{h,Ca}$	-48.9	fitted
	$\tau_{m,Ca}$	300 ms	$V_{m,Ca}$	-27.3 mV	
	$k_{h,Ca}$	-18.2	$k_{m,Ca}$	4.62 mV	
	g_{Ca}	2.1 nS (2.8 nS in OVX+E2)	E_{Ca}	121.6 mV	
I_{TRPC5}	c_{TRPC5}	0.6 µM	k_{TRPC5}	0.33 µM	[11]
	$k_{R_{TRPC5}}$	0.006 ms^{-1}	$k_{-R_{TRPC5}}$	0.002 ms^{-1}	
	$k_{R_{TRPC5},0}$	0.002 ms^{-1}	g_{TRPC5}	8.4 nS (1.68 nS in OVX+E2)	
	K_{NKB}	32 µM	$n2$	2	
	$R_{TRPC5,T}$	1 µM	E_{TRPC5}	-15 mV	
I_{GIRK}	V_{GIRK}	-70 mV	$k_{GIRK,1}$	20 mV	[12]
	α	0.8	α_τ	0.0061	
	$k_{GIRK,2}$	100 mV	β_τ	0.0818	
	g_{GIRK}	0.4 nS	E_K	-81 mV	
	$k_{R_{GIRK},0}$	0 ms^{-1}	$k_{R_{GIRK}}$	10^{-3} ms^{-1}	
	$R_{GIRK,T}$	1 µM	K_S	1 µM	
	$k_{-R_{GIRK}}$	$3.3 \cdot 10^{-6}$ ms^{-1}	$n3$	2	
I_{leak}	$g_{leak,1}$	3.5 nS in OVX 3.65 nS in OVX+E2	$g_{leak,2}$	4 nS	fitted
Intracellular calcium					
	γ	$1.96 \cdot 10^{-5}$ µM nA^{-1} ms^{-1}	d_{ca}	0.008 ms^{-1}	[6]

Table S1 Table of model parameters.

References

1. Fry, M., Boegle, A.K. and Maue, R.A. 2007. Differentiated pattern of sodium channel expression in dissociated Purkinje neurons maintained in long-term culture. *Journal of Neurochemistry* **101**:737-748. PMID: 17448145.

2. Zhang, C., Bosch, M.A., Qiu, J., Ronnekleiv, O.K. and Kelly, M.J. 2015. 17β-Estradiol increases persistent Na^+ current and excitability of AVPV/PeN Kiss1 neurons in female mice. *Molecular Endocrinology* **29**:518-527. PMID: 25734516.

3. Moran, S., Moenter, S.M. and Khadra, A. 2016, A unified model for two modes of bursting in GnRH neurons. *Journal of Computational Neuroscience* **40**, 297-315. PMID: 26975615.

4. Mendonça, P.R., Vargas-Caballero, M., Erdelyi, F., Szabo, G., Paulsen, O. and Robinson, H.P. 2016. Stochastic and deterministic dynamics of intrinsically irregular firing in cortical inhibitory interneurons. *eLife* **5**:e16475. PMID: 27536875.

5. Mendonça, P.R., Kyle, V., Yeo, S.H., Colledge, W.H. & Robinson, H.P. 2018. Kv4. 2 channel activity controls intrinsic firing dynamics of arcuate kisspeptin neurons. *The Journal of Physiology* **596**:885-899. PMID: 29214635.

6. Tsaneva-Atanasova, K., Sherman, A., Goor, F.v. and Stojilkovic, S.S. 2007. Mechanism of spontaneous and receptor-controlled electrical activity in pituitary somatotrophs: experiments and theory. *Journal of Neurophysiology* **98**:131-144. PMID: 17493919.

7. Booth, C.A., Witton, J., Nowacki, J., Tsaneva-Atanasova, K., Jones, M.W., Randall, A.D., Brown, J.T. 2016. Altered intrinsic pyramidal neuron properties and pathway-specific synaptic dysfunction underlie aberrant hippocampal network function in a mouse model of tauopathy. *Journal of Neuroscience* **13**:350-63. PMID: 26758828.

8. Conde, K. and Roepke, T. 2020. 17β-estradiol increases arcuate KNDy neuronal sensitivity to ghrelin inhibition of the M-current in female mice. *Neuroendocrinology* **110**:582-594. PMID: 31484184.

9. Nowacki, J., Osinga, H.M., Brown, J.T., Randall, A.D. & Tsaneva-Atanasova, K. 2011. A unified model of CA1/3 pyramidal cells: An investigation into excitability. *Progress in Biophysics and Molecular Biology* **105**:34-48. PMID: 20887748.

10. Wang, L., DeFazio, R.A. and Moenter, S.M. 2016. Excitability and burst generation of AVPV kisspeptin neurons are regulated by the estrous cycle via multiple conductances modulated by estradiol action. *eNeuro* **3**, e0094-0016.2016. PMID: 27280155.

11. Qiu, J., Stincic, T.L., Bosch, M.A., Connors, A.M., Petrie, S.K., Rønnekleiv, O.K. and Kelly, M.J. 2021. Deletion of Stim1 in hypothalamic arcuate nucleus Kiss1 neurons potentiates synchronous GCaMP activity and protects against diet-induced obesity. *Journal of Neuroscience* **41**:9688-9701. PMID: 34654752.

12. Tian, J.-b., Yang, J., Joslin, W.C., Flockerzi, V., Prescott, S.A., Birnbaumer, L. and Zhu, M.X. 2022.TRPC4 and GIRK channels underlie neuronal coding of firing patterns that reflect $G_{q/11}$ - $G_{i/o}$ coincidence signals of variable strengths. *Proceedings of the National Academy of Sciences* **119**:e2120870119. PMID: 35544691

13. Bond, C.T., Maylie, J., Adelman, J.P. 1999. Small-conductance calcium-activated potassium channels. *Annals of New York Acadamy of Sciences*. **868**:370-8. PMID: 10414306.

14. Gottsch, M.L., Popa, S.M., Lawhorn, J.K., Qiu, J., Tonsfeldt, K.J., Bosch, M.A., Kelly, M.J., Rønnekleiv, O.K., Sanz, E., McKnight, G.S., Clifton, D.K., Palmiter, R.D. and Steiner, R.A. 2011. Molecular properties of Kiss1 neurons in the arcuate nucleus of the mouse. *Endocrinology* **152**:4298-4309. PMID: 21933870.

15. Qiu, J., Rivera, H.M., Bosch, M.A., Padilla, S.L., Stincic, T.L., Palmiter, R.D., Kelly, M.J. and Rønnekleiv, O.K. 2018. Estrogenic-dependent glutamatergic neurotransmission from kisspeptin neurons governs feeding circuits in females. *eLife* **7**:e35656. PMID: 30079889.